JOURNAL OF PETROLOGY | VOLUME 45 | NUMBER 6 | PAGES 1237–1259 | 2004 | DOI: 10.1093/petrology/egh012

Quantitative Constraints on Metamorphism in the Variscides of Southern Brittany—a Complementary Pseudosection Approach

TIM JOHNSON AND MICHAEL BROWN*

LABORATORY FOR CRUSTAL PETROLOGY, DEPARTMENT OF GEOLOGY, UNIVERSITY OF MARYLAND, COLLEGE PARK, MD 20742-4211, USA

RECEIVED JUNE 19, 2003; ACCEPTED DECEMBER 11, 2003

Previous studies of metapelitic rocks from the core of the southern Brittany metamorphic belt suggest a complex clockwise P–T *evolution. We use pseudosections calculated for an average subaluminous metapelite composition in the MnNCKFMASH system and average* P–T *calculations to investigate in more detail the metamorphic evolution of these rocks. For migmatites, sequential occurrence of kyanite, kyanite + staurolite and sillimanite suggests that a prograde evolution to* $P > 8$ *kbar at* $T \approx 625°C$ *was followed by a* P *decrease to around 6 kbar at 650°C. Subsequent heating and burial led to melting as a result of the incongruent breakdown of first muscovite then biotite; at the metamorphic peak (*$P \approx 8$ *kbar,* $T \approx 800°C$*), around 25 mol % melt and >20 mol % garnet are predicted. The retrograde evolution began with conductive cooling, allowing crystallization of melt and retrograde replacement of garnet by reaction to biotite and sillimanite. Subsequent near-isothermal decompression from around* $P \approx 6$ *kbar to* $P \approx 4$ *kbar was associated with widespread development of cordierite and a second episode of melt generation. Microstructural relations in upper amphibolite-facies metapelites from the unit structurally overlying the migmatites are consistent with growth of staurolite, andalusite and white mica along the retrograde path. On the basis of phase relations that account for the quantity of* H_2O *required to saturate a given assemblage, an influx of an* H_2O*-rich volatile phase is implied, which we infer to have been derived from crystallizing melt in underlying granites. The close correspondence of predictions from pseudosections to thermobarometric results is encouraging, and the complementary approach used has allowed tighter constraints than before to be placed on the* P–T–X *evolution of this sector of the Variscides.*

KEY WORDS: *melting; pseudosections;* P–T *path; retrograde metamorphism; Variscan*

INTRODUCTION

The Earth's crust is formed and modified by magmatism and orogenesis, and recycled by erosion, sedimentation and metamorphism; rocks preserve a record of these processes in their structural relationships, bulk-rock chemistry, microstructures, mineral assemblages and mineral chemistry. The record is commonly only partially complete, as a result of erasure during overprinting or structural reworking, and may be better preserved in some rocks than in others; parts of the record may be cryptic. These factors limit our ability to unravel the rock record.

Many of the inverse methods used in petrology (e.g. thermobarometry) are based on an assumption of equilibrium on some length scale in some time frame; this implies continuous overprinting of mineral assemblages, and change in mineral proportions and compositions during monocyclic evolution or thorough structural reworking and resetting during polycyclic evolution. Commonly, this assumption is considered reasonable in circumstances where a volatile phase or melt is present. In addition to the inverse approach, forward modelling provides a potentially powerful tool to evaluate alternative hypotheses in order to distinguish those that reproduce preserved elements of the rock record from alternatives that generate conflicts with these data.

Hensen (1971) introduced the use of equilibrium phase diagrams that represent paragenetic relations for a specified composition in a defined system in terms of two intensive variables (pseudosections) to investigate the stability of garnet–cordierite parageneses in metapelitic rocks. He used *P*–*T* pseudosections to display the

*Corresponding author. Telephone: +1 301 405 4080. Fax: +1 301 314 7970. E-mail: mbrown@geol.umd.edu

position and extent of divariant reactions, and their relationship to the stable sections of univariant reactions, in the model system FMAS ($FeO-MgO-Al_2O_3-SiO_2$). Subsequently, these projections have proven useful in forward modelling of the $P-T$ evolution of particular rocks (e.g. Pattison & Tracy, 1991). Use of such diagrams also led to the realization that univariant reactions are rarely intersected by individual rocks of fixed bulk composition during passage through an orogen, even in simple systems.

As experimental and thermodynamic data for a wider range of compositional end-members have become available (Holland & Powell, 1998), and expressions for activity–composition relations in multi-component systems have improved (e.g. Holland & Powell, 1996*a*, 1996*b*, 2003), so model systems have become increasingly more complex and more closely approximate natural rocks (e.g. Guiraud *et al.*, 2001; White *et al.*, 2001, 2002; Johnson *et al.*, 2003*a*), so that today pseudosections are constructed for an ever larger range of compositions (e.g. Carson *et al.*, 1999; White *et al.*, 2000) for various combinations of intensive parameters (P, T, X, aH_2O, etc.). Pseudosections allow quantitative investigation of processes, including volatile phase infiltration, melt loss and scales of equilibrium (Stüwe, 1997; Marmo *et al.*, 2002; White & Powell, 2002; Johnson *et al.*, 2003*b*).

The use of pseudosections to evaluate the stability of mineral assemblages and evolution from one assemblage to another has become increasingly common (e.g. Tinkham *et al.*, 2001; White *et al.*, 2001, 2002; Johnson *et al.*, 2003*a*, 2003*b*; Kelsey *et al.*, 2003*a*, 2003*b*; Zeh & Holness, 2003). The reason underlying this increased use is the desire to make quantitative predictions about the multivariant stability fields of paragenetic associations for both inverse and forward modelling of particular metamorphic rocks. In this study, we use both inverse methods and forward modelling of well-constrained microstructural relations and mineral assemblages to investigate, in a quantitative manner, the metamorphic evolution of high-grade subsolidus and suprasolidus (migmatitic) metapelitic rocks in southern Brittany, in the Armorican Massif of western France, part of the European Variscides. Detailed investigations of the rocks discussed have been undertaken by Brown (1983), Triboulet & Audren (1985, 1988), Jones & Brown (1989, 1990), Audren & Triboulet (1993) and Brown & Dallmeyer (1996); here we summarize only those aspects of relevance to the current study. Using new and extant mineralogical and microstructural data, we compare previous interpretations of the $P-T-t-d$ path inferred for the rocks with pseudosections constructed in the MnNCKFMASH ($MnO-Na_2O-CaO-K_2O-FeO-MgO-Al_2O_3-SiO_2-H_2O$) model system.

GEOLOGICAL SETTING

The Armorican Massif of France forms part of the Ibero-Armorican Arc, a major syntaxis of the Variscan belt of Western Europe (e.g. Ballèvre *et al.*, 1992). It comprises several tectonometamorphic domains separated by major shear zones active during the Variscan that record dextral strike-slip displacement. The North Armorican shear zone (NASZ) and South Armorican shear zone (SASZ) separate the Massif into the North Armorican Composite Terrane, Central Armorica and South Armorica (Fig. 1, inset). The North Armorican Composite Terrane is essentially of late Precambrian origin; it behaved as a brittle domain during Variscan deformation. Central Armorica comprises Neoproterozoic to Carboniferous detrital sedimentary rock successions that were only moderately thickened and affected by low-grade (anchizone to greenschist-facies) metamorphism during pervasive Variscan dextral strike-slip deformation (Gapais & Le Corre, 1980). South Armorica forms the internal zone of the Variscan orogenic belt; it is composed of two main groups of tectonostratigraphic units that together form the southern Brittany metamorphic belt.

Units equilibrated at lower-crustal depths are the Vilaine Group (Fig. 1) and the structurally lower southern Brittany migmatite belt (SBMB; Fig. 1); they are characterized by high-T–moderate-to-low-P metamorphism associated with the late Variscan extensional deformation that followed peak metamorphism in crust thickened during the terminal phase of Variscan subduction and continental collision (e.g. Brun & Burg, 1982; Matte & Hirn, 1988; Jones, 1991; Matte, 1991, 2001; Burg *et al.*, 1994; Cagnard *et al.*, 2004). The Belle-Ile group (Fig. 1) represents an upper-crustal domain during the late Variscan (Late Carboniferous) evolution; it is composed of units characterized by high-P–low-T metamorphism associated with subduction and exhumation during the early Variscan evolution (Late Devonian to Early Carboniferous; Ballèvre *et al.*, 2003*a*).

The SBMB is largely composed of high-grade, migmatized metasedimentary rocks and anatectic granites, with subordinate layers of amphibolite and Ordovician orthogneisses (e.g. Brown, 1983; Jones & Brown, 1990; Audren & Triboulet, 1993). The Vilaine Group is dominated by largely unmigmatized interbedded metaclastic and meta-tuffaceous rocks with amphibolite horizons; it records uppermost amphibolite-facies metamorphism around the Vilaine estuary (e.g. Triboulet & Audren, 1985, 1988), but in Vendée the metamorphic grade decreases upward through the group (e.g. Bossière, 1988; Goujou, 1992). The lower part of the Belle-Ile Group is characterized by highly strained, low-grade siliceous metavolcanic and metavolcaniclastic rocks (the Vendée porphyroids) and metapelites (e.g. Audren & Plaine, 1986; Le Hébel *et al.*, 2002*a*; Schultz *et al.*, 2002);

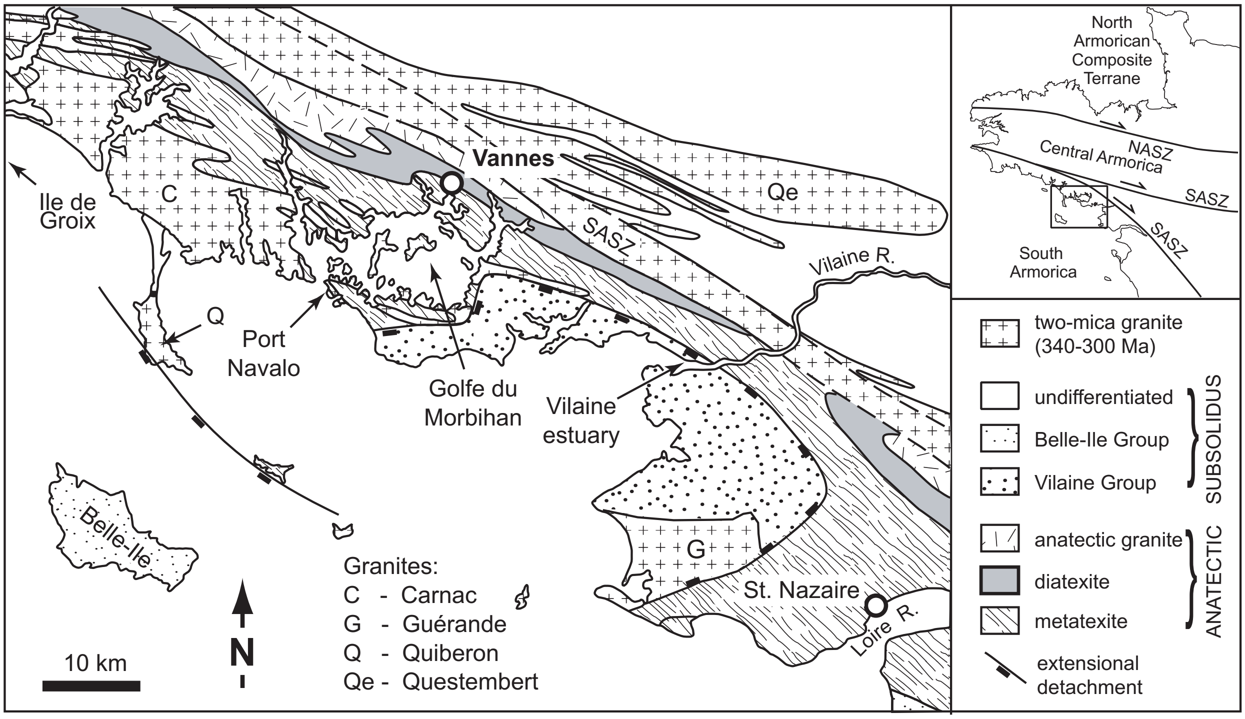

Fig. 1. Geological map of the Golfe du Morbihan–Vilaine estuary–St. Nazaire region of the southern Brittany metamorphic belt showing study locations. The inset shows the regional context of the study area. Modified after Gapais *et al.* (1993) and Marchildon & Brown (2003).

these rocks record moderate-*P*–low-*T* metamorphism (Le Hébel *et al.*, 2002*b*). Apparently overlying these units are the blueschist rocks and eclogites of oceanic affinity exposed on the Ile de Groix and in the Bois de Cené (e.g. Quinquis & Choukroune, 1981; Bernard-Griffiths *et al.*, 1986; Shelley & Bossière, 1999; Schultz *et al.*, 2001); these rocks record high-*P*–low-*T* metamorphism (Triboulet, 1974, 1991; Guiraud *et al.*, 1987; Djro *et al.*, 1989; Bosse *et al.*, 2002; Ballèvre *et al.*, 2003*b*). Contacts between units are shallow, with the Belle-Ile Group generally separated from the underlying high-grade rocks by two-mica leucogranite in shallow-dipping tabular plutons that mark extensional ductile shear zones (Gapais *et al.*, 1993; Brown & Dallmeyer, 1996). The overall structural architecture defines windows of high-*T*–low-*P* rocks that represent structural culminations surrounded by the high-*P*–low-*T* units in structural depressions (Fig. 1).

Recent work on the porphyroids and blueschists of the Belle-Ile Group indicates that the peak of high-*P*–low-*T* metamorphism was at 370–360 Ma, with exhumation and cooling *c.* 350 Ma (e.g. Bosse *et al.*, 2000; Le Hébel, 2002). There is no evidence of a Late Carboniferous low-*P*–high-*T* metamorphic overprint in these rocks, in contrast to the metamorphic history in the eastern Variscides (e.g. Brown & O'Brien, 1997). However, geochronological data from the migmatites, Vilaine Group rocks and anatectic granites of the Golfe du Morbihan and Vilaine estuary region suggest a rapid evolution in the Late Carboniferous, as age data on monazite (U–Pb), hornblende ($^{40}Ar/^{39}Ar$), mica (Rb–Sr and $^{40}Ar/^{39}Ar$), and apatite (fission tracks) all lie in the range 320–290 Ma (Brown & Dallmeyer, 1996).

In summary, the tectonometamorphic evolution of South Armorica is composed of two principal stages: a Late Devonian to Early Carboniferous high-*P*–low-*T* stage that involved thrusting and piling up of nappes during a subduction to continental collision transition, followed by a Late Carboniferous high-*T* metamorphism that is associated with granite magmatism. The second stage is inferred to be related to regional extension.

FIELD RELATIONS AND PETROGRAPHY OF ROCKS OF THE VILAINE ESTUARY AND MIGMATITES OF THE GOLFE DU MORBIHAN AND ST. NAZAIRE

In this study, we concentrate on the metamorphic evolution of rocks from the late Variscan lower-crustal domain, which complements recently published interpretations of the metamorphism of rocks of the overlying Belle-Ile Group (Schultz *et al.*, 2001; Bosse *et al.*, 2002; Le Hébel, 2002; Le Hébel *et al.*, 2002*a*, 2002*b*; Ballèvre *et al.*, 2003*b*). Samples used in this study come from the Vilaine estuary, and the Golfe du Morbihan and St. Nazaire regions (Fig. 1).

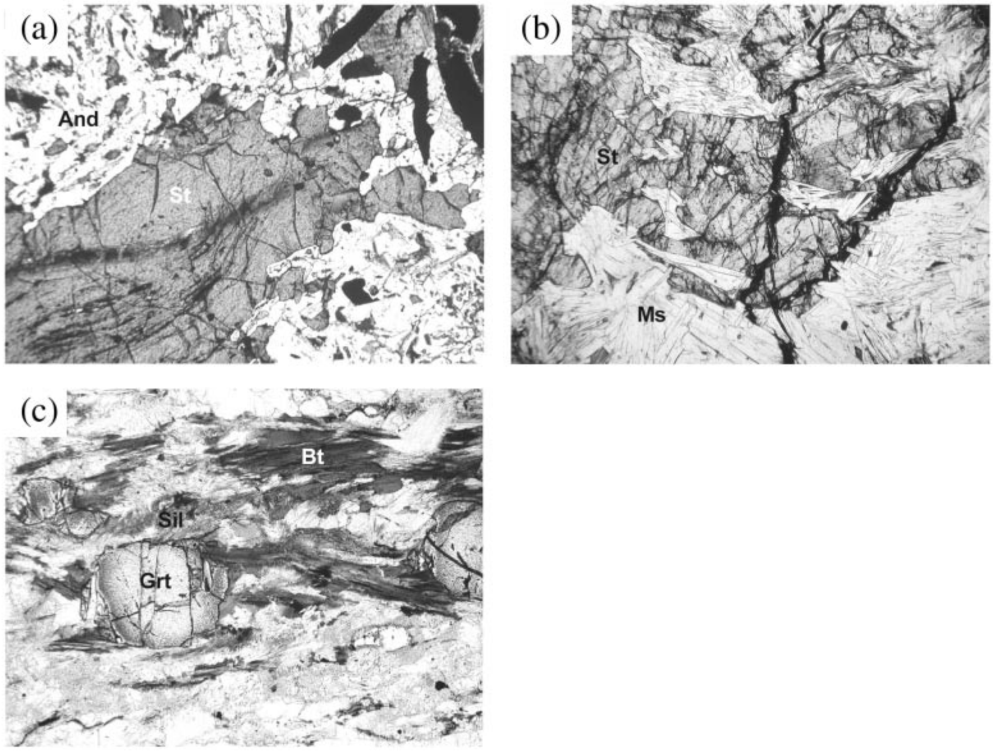

Fig. 2. Petrographic aspects of metapelitic rocks from the Vilaine estuary. (a) Corroded staurolite replaced by andalusite and biotite. Fine graphite inclusions define a weakly crenulated schistosity, supporting relatively late growth of staurolite (syn-D_2; Triboulet & Audren, 1985). Long dimension of photomicrograph is 2·5 mm. (b) Staurolite surrounded by decussate phengitic white mica, inferred to be a replacement product after andalusite and biotite. Long dimension of photomicrograph is 3 mm. (c) Garnet within staurolite-absent layers, associated with fabric-forming biotite and fibrolitic sillimanite. Long dimension of photomicrograph is 2 mm.

In the Golfe du Morbihan (Fig. 1), a sharp contact is inferred between rocks of the SBMB and those of the Belle-Ile Group, marked by the mylonitized Quiberon granite that was emplaced during normal-slip shear. The overall geometry is one of an extensional detachment (Gapais *et al.*, 1993), beneath which the main foliation in the migmatites is steeply dipping. The migmatites are cut by steeply dipping dykes of granite that indicate east–west extension (Audren, 1987). The steep attitude of the main foliation in the migmatites could have been acquired during passive rise of the SBMB (Tirel *et al.*, 2003), synchronous with dextral strike-slip displacement along the SASZ and pervasive dextral shear deformation in the migmatites (Marchildon & Brown, 2003). In the Vilaine estuary, exhumation is inferred to be coeval among the Vilaine Group rocks and the SBMB, based on similar $^{40}Ar/^{39}Ar$ ages on hornblende from amphibolite in both groups (Brown & Dallmeyer, 1996). This implies a common element in the late stage of the metamorphic evolution of both groups, even though the contact between the two groups also is marked by two-mica granites (Sarzeau granite—Audren, 1987; Guérande granite—Bouchez *et al.*, 1981; Fig. 1).

Metamorphic studies on amphibolite-facies rocks of the Vilaine Group (Triboulet & Audren, 1985, 1988) and migmatites within the SBMB (Brown, 1983; Jones & Brown, 1990; Audren & Triboulet, 1993; Brown & Dallmeyer, 1996), which combine macro- and microstructural observations, inferred stable paragenetic associations, mineral chemistry, conventional thermobarometry and geochronology, have allowed characterization of the tectonometamorphic evolution of the belt. The results suggest that the rocks followed a clockwise P–T–t–d path that involved significant post-peak exhumation and consequent decompression (e.g. Jones & Brown, 1990; Audren & Triboulet, 1993).

Amphibolite-facies metapelitic rocks of the Vilaine estuary

Rocks cropping out along the margins of the Vilaine estuary (Fig. 1) comprise fine- to medium-grained, strongly foliated metapelites, some containing all three Al_2SiO_5 polymorphs. The lowest variance assemblages contain biotite, garnet, staurolite, sillimanite (after kyanite?), andalusite, white mica and quartz. Variably corroded staurolite grains are mantled by andalusite and biotite (Fig. 2a) or phengitic white mica (Fig. 2b). Crenulated trails of graphite inclusions (Fig. 2a) support the interpretation that staurolite grew late in the deformation sequence (syn-D_2; Triboulet & Audren, 1985). Localized greenschist-facies retrograde reaction (and volatile phase influx) is evident from marginal alteration of garnet and biotite to chlorite, and partial to complete replacement of andalusite by white mica (Fig. 2b). The inferred reaction succession kyanite → sillimanite → andalusite is consistent with chemical zonation in solid solution phases, principally garnet and staurolite, which together imply a clockwise P–T–t evolution (Triboulet & Audren, 1985). Staurolite-free metapelitic rocks may contain kyanite and/or orthoclase with subhedral to euhedral, commonly unresorbed garnet (Fig. 2c). Cordierite is not reported from these rocks.

Migmatites of the Golfe du Morbihan and St. Nazaire

Within the SBMB, migmatites that crop out around the Golfe du Morbihan and at St. Nazaire (Fig. 1) are stromatic metatexites with irregular podiform and tabular bodies of diatexite (Jones & Brown, 1990). The rocks record a complex sequence of melt-present polyphase deformation, reflected by three principal folding events and transposed foliations (Audren, 1987; Jones, 1991; Marchildon & Brown, 2003). Garnet is common and occurs both within mesosome (consistent with subsolidus growth) and leucosome (consistent with suprasolidus/peritectic growth). Primary muscovite is absent and retrograde muscovite is rare. Characteristic lithologies include blue–grey sillimanite- and cordierite-rich gneiss (morbihanite) and rare coarse-grained garnet–cordierite gneiss, both of which are well exposed at Port Navalo and SW of St. Nazaire (Fig. 1).

Garnet–cordierite gneiss preserves the most complete evidence for the P–T–t evolution of the rocks (Jones & Brown, 1990). Garnet porphyroblasts, up to 10 mm in diameter, have inclusion-rich cores and, in the largest, least retrogressed examples, inclusion-poor rims (Fig. 3a). Zones with different inclusion suites include an inner core containing kyanite (with ilmenite and quartz) and an outer core containing staurolite (and rutile with kyanite or sillimanite; Fig. 3b) and sillimanite (with or without rutile). Garnet exhibits replacement by coarse-grained aggregates of biotite and sillimanite, with plagioclase and quartz (Fig. 3a). Such replacement suggests retrograde reaction with melt, although the preservation of garnet is consistent with net melt loss (e.g. Powell & Downes, 1990). These partially replaced garnets are surrounded by a mantle of cordierite, most of which has partially replaced retrograde biotite and sillimanite (Fig. 3a and c); rare spinel–cordierite symplectites after sillimanite occur in silica-deficient domains (Fig. 3c), consistent with decompression. Fabric-forming biotite commonly shows replacement by cordierite (Fig. 3d); prismatic sillimanite exhibits ubiquitous replacement by cordierite, with sillimanite isolated from all other phases (Fig. 3e).

Morbihanite is characterized by abundant sillimanite, which exhibits ubiquitous replacement by cordierite. Discrete leucosomes generally lack a biotite-rich selvage, a feature common in the other migmatites. Euhedral to subhedral peritectic garnet occurring within leucosome veins is commonly unaltered, consistent with net melt loss from these domains (e.g. Johnson *et al.*, 2003*b*). Whereas the garnet–cordierite gneiss preserves the most complete record of the tectonothermal evolution of the rocks, similar reaction microstructures are preserved in metatexite, diatexite and morbihanite. In leucosomes of all samples, compositionally zoned plagioclase grains, interpreted to be magmatic, contain relics of kyanite, suggesting this was the stable Al_2SiO_5 polymorph at the onset of major melting by volatile phase-absent muscovite breakdown. Paragenetic and microstructural relations are consistent with a clockwise P–T evolution involving late high-T decompression (Brown, 1983; Jones & Brown, 1989, 1990; Audren & Triboulet, 1993; Brown & Dallmeyer, 1996). Decompression is particularly marked in the migmatites by cordierite that occurs as inclusion-poor, subhedral grains with minimal leucosome in interboudin partitions (Fig. 3f). This cordierite is interpreted as a peritectic product of biotite-consuming melting reactions, implying a second (low-P) stage of melt generation.

GARNET ZONATION

Compositional zoning of major elements in garnet (Fe, Mg, Ca, Mn) was investigated qualitatively and quantitatively using X-ray intensity maps and single spot analyses along radial traverses, respectively. Data were collected using the JEOL JXA-8900 SuperProbe at the Center for Microanalysis and Microscopy, University of Maryland. Operating conditions for map collection used a 5 μm beam diameter, a beam current of 200–250 nA and dwell times of 200 ms. For spot analyses, operating conditions were 15 kV and 20 nA, with a beam diameter of 5 μm. Natural materials were used as standards.

Garnet was studied in detail from samples of amphibolite-facies metapelite from the Vilaine estuary, and garnet–cordierite gneiss and morbihanite from Port Navalo (Fig. 1). Multiple garnet grains from all samples were investigated to ensure that data presented in Fig. 4 are representative. Figure 4 shows major element maps and quantitative compositional profiles for representative garnets from these samples. The colour contrast on the maps was adjusted to best highlight compositional inhomogeneity for the element in question, as absolute variations in concentration are generally small.

Garnet from metapelite of the Vilaine estuary

The selected garnet occurs within a staurolite-absent quartzofeldspathic layer in which garnets are subhedral,

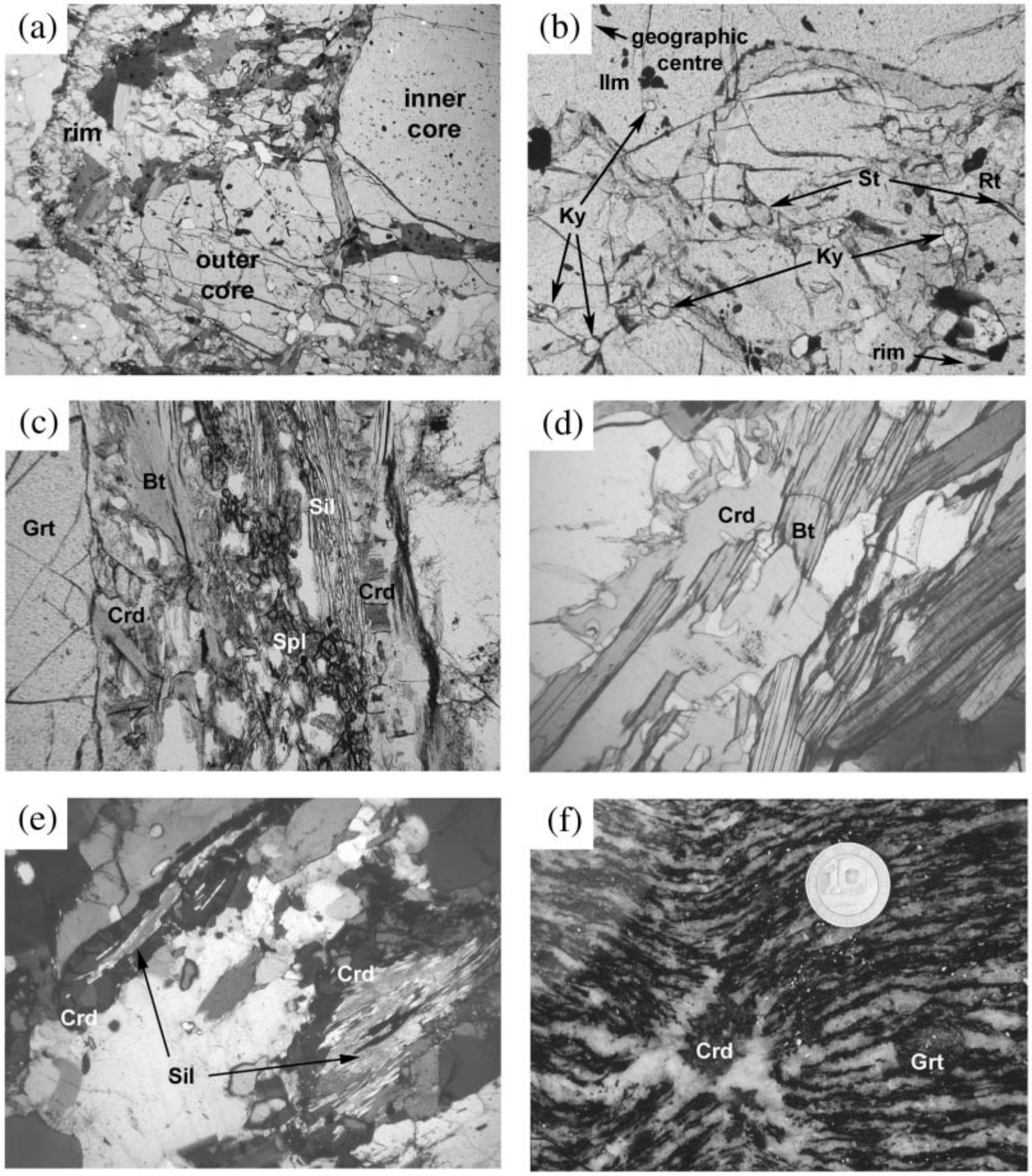

Fig. 3. Petrographic aspects of the migmatites from the Golfe du Morbihan and St. Nazaire. (a) Partially replaced garnet. The outer regions of the unaltered inner core contain inclusions of kyanite. The partially replaced outer core contains inclusions of staurolite and kyanite. The rim shows pseudomorphic replacement by cordierite, biotite and plagioclase, and quartz. Garnet–cordierite gneiss, Port Navalo, Golfe du Morbihan; long dimension of field of view is 6 mm. (b) Inclusion suite within a 10 mm diameter garnet. The inner core (left) contains inclusions of kyanite (+ ilmenite); the outer core (right) has inclusions of staurolite + kyanite (+ rutile). The direction to the geographical centre (interpreted to be close to the earliest grown garnet) and biotite-rich, partially replaced rim are indicated. Garnet–cordierite gneiss, St. Nazaire; long dimension of field of view is 2·5 mm. (c) Rim of large garnet showing replacement by cordierite, biotite and prismatic sillimanite against leucosome. Sillimanite-rich areas show subsequent replacement by symplectic intergrowths of spinel + cordierite, indicative of decompression. Stromatic migmatite (metatexite), Port Navalo, Golfe du Morbihan; long dimension of field of view is 1·5 mm. (d) Partial replacement of matrix biotite by pinitized cordierite. Stromatic migmatite (metatexite), Port Navalo, Golfe du Morbihan; long dimension of field of view is 1 mm. (e) Sillimanite replaced by cordierite. This microstructure is ubiquitous, suggesting that sillimanite was not part of the stable assemblage during the latter stages of retrograde reaction. Morbihanite, Port Navalo, Golfe du Morbihan; long dimension of field of view is 2·5 mm. (f) Large inclusion-poor grains of pinitized cordierite within leucosome-filled interboudin partition, interpreted to represent small degrees of late-stage decompression melting. A large, partially replaced garnet is shown towards the bottom right. Wave-cut platform, Port Navalo, Golfe du Morbihan; 1 euro coin gives scale.

generally <1 mm in diameter and contain small inclusions throughout (e.g. Fig. 4a). Zoning is continuous from core to rim. Cores are enriched in Mg [X_{Py} = 0·10–0·11, where X_{Py} = Mg/(Mg + Fe + Mn + Ca)] and Fe (X_{Alm} = 0·68–0·70), and depleted in Mn (X_{Sps} = 0·14) relative to the rim (X_{Py} = 0·07; X_{Alm} = 0·65; X_{Sps} = 0·24–0·25). Ca concentrations are higher in the core (0·07) than in the rim (0·03–0·04), although higher values

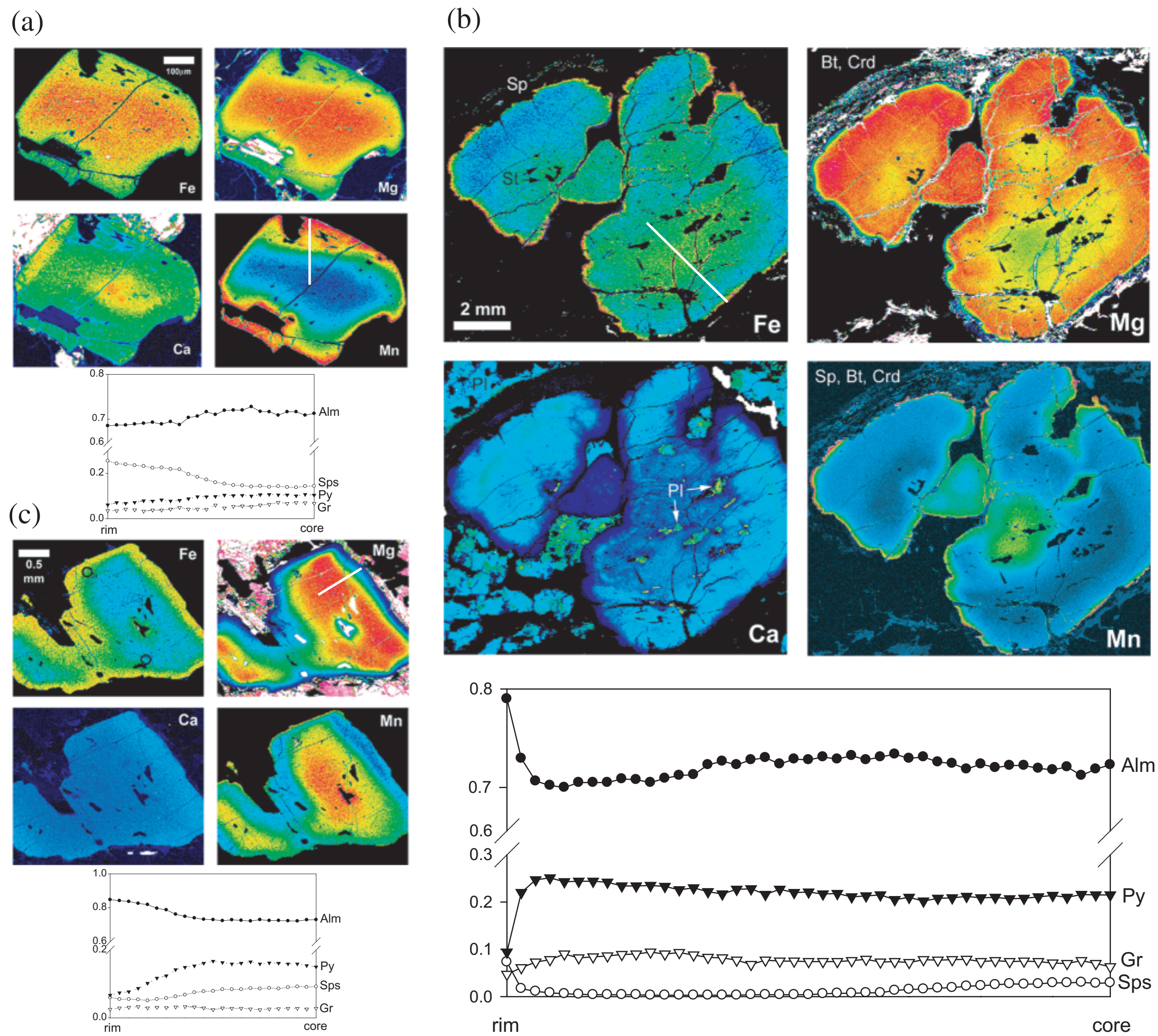

Fig. 4. X-ray compositional maps and quantitative core to rim spot analyses of garnet from: (a) a staurolite-free layer within a metapelitic rocks from the Vilaine estuary; (b) a garnet–cordierite gneiss; (c) a sample of morbihanite. (b) and (c) from Port Navalo. The results are discussed in detail within the text.

are recorded where garnet is in contact with matrix plagioclase.

Garnet from garnet–cordierite gneiss at Port Navalo, Golfe du Morbihan

The garnet shown in Fig. 4b was selected for its large size (around 10 mm) and minimal marginal replacement by retrograde minerals. The garnet comprises an inclusion-rich core with a 1–2 mm wide inclusion-poor rim (Fig. 4b). The magnesium content exhibits continuous zoning from core to rim. Cores are relatively depleted in the pyrope component ($X_{Py} = 0{\cdot}21$–$0{\cdot}22$), with contents increasing towards the rim; the highest concentrations ($X_{Py} = 0{\cdot}25$) occur close to the outer edge of the grain, within the inclusion-poor portion. A thin outermost rim (0·2–0·3 mm), where garnet is in contact with the matrix, is characterized by a marked decrease in magnesium content (to $X_{Py} = 0{\cdot}09$; Fig. 4b). Fe exhibits smooth zoning that varies antipathetically with that of Mg ($X_{Alm} = 0{\cdot}69$ in the core, 0·66 in the wide rim, 0·79 in the outermost rim). Mn exhibits most compositional complexity although variations are subtle. The innermost core, enriched in spessartine ($X_{Sps} = 0{\cdot}029$), corresponds to the low-Mg core. Mn concentrations decrease rimwards, the lowest values ($X_{Sps} = 0{\cdot}003$) occurring at the boundary between the inclusion-rich core and the inclusion-poor rim (Fig. 4b). The rim has broadly constant Mn contents ($X_{Sps} = 0{\cdot}004$–$0{\cdot}006$) except at the extreme edge, where spessartine contents are highest (X_{Sps} = 0·095). The core (X_{Gr} = 0·07–0·08) is relatively depleted in Ca compared with the patchily zoned rim (X_{Gr} = 0·08–0·09), although the boundary between the two does not correspond precisely to that defined by Mg and Mn distributions (see Spear & Daniel, 2001). Garnet is Ca depleted where in contact with plagioclase and surrounding plagioclase inclusions; the lowest X_{Gr} values are around 0·05.

Garnet from morbihanite at Port Navalo, Golfe du Morbihan

The garnet selected is around 2 mm in diameter and contains inclusions of biotite. The zoning profile is smooth and continuous from core to rim, although profiles for all elements are inflected (Fig. 4c). Both Mn and Mg are enriched in the core (X_{Py} = 0·15–0·16; X_{Sps} = 0·09) relative to the rim (X_{Py} = 0·07–0·08; X_{Sps} = 0·06) and vary antipathetically with Fe (X_{Alm} = 0·72–0·73 in the core, 0·84–0·85 in the rim). Fe and Mg concentrations increase and decrease respectively where garnet is in contact with biotite inclusions. Ca shows very little variation (X_{Gr} around 0·03). Compositional maps for a small (0·5 mm) inclusion-free garnet occurring within a thin stromatic leucosome show that major elements are essentially unzoned and there is no marginal retrograde replacement of garnet.

THERMOBAROMETRY

Metapelite of the Vilaine estuary

Triboulet & Audren (1985) calculated P–T conditions in metapelitic rocks from the Vilaine estuary using garnet–biotite Fe–Mg exchange thermometry (in staurolite-absent assemblages) and garnet–Al-silicate–quartz–plagioclase (GASP) barometry. Their results suggest that peak pressures of 8–9 kbar at 580°C preceded the metamorphic peak at $T \approx 640$°C, $P \approx 7$ kbar, consistent with the high-T sillimanite-bearing assemblages developed. Decompression to $P \approx 4$ kbar, $T \approx 540$°C is inferred from the retrograde development of staurolite and its subsequent replacement by andalusite. Calculations based on the breakdown of paragonite + quartz to albite + Al-silicate + H_2O suggest a reduced activity of H_2O in the volatile phase (Triboulet & Audren, 1985), consistent with the presence of graphite (Fig. 2a). Chemical zonation of amphibole inferred to have been in equilibrium with plagioclase, chlorite, epidote, quartz and an assumed volatile phase within interbedded magnesian metabasite layers yields results that are consistent with those from the metapelites, implying the rocks shared a common tectonometamorphic history (Triboulet & Audren, 1988).

Migmatites of the Golfe du Morbihan and St. Nazaire

Jones & Brown (1990) calculated P–T conditions in migmatites from locations around the Golfe du Morbihan and close to St. Nazaire for prograde, peak and retrograde metamorphism using garnet–staurolite, garnet–biotite and garnet–cordierite Fe–Mg exchange thermometry and barometers based on the GASP and garnet–rutile–Al-silicate–ilmenite–quartz (GRAIL) net-transfer equilibria. Their calculations implied that peak metamorphic conditions of $P \approx 8$ kbar, $T \approx 800$°C were superseded by retrograde decompression to $P \approx 4$ kbar, $T \approx 700$°C. Brown & Dallmeyer (1996) used hornblende and muscovite $^{40}Ar/^{39}Ar$ ages in combination with published ages on monazite, biotite and apatite to show that subsequent cooling was rapid (14 ± 4°C/Ma).

Using the mineral chemistry data of Jones & Brown (1990), we have recalculated the results for the SBMB using the average P–T mode of THERMOCALC (Powell & Holland, 1994) to incorporate recent activity–composition models (Tables 1 and 2). This approach has the advantage of making the results consistent with pseudosections used in subsequent discussion. Calculations to determine peak metamorphic conditions use garnet core/peak compositions and proximal inclusions; calculations to determine retrograde metamorphic conditions use inclusion-poor garnet rims and proximal matrix phases (Jones & Brown, 1990).

Given the evidence that both the high-T prograde and retrograde evolution occurred in the presence of melt, the results are dependent on the volatile content in cordierite. Calculations assume a volatile-undersaturated system with a fixed aH_2O in cordierite of 0·4, a value that is at the high end of the range of measurements in cordierite from migmatites inferred to have resulted from volatile phase-absent melting of metapelite (Harley & Carrington, 2001). Calculated temperatures are essentially independent of the volatile content in cordierite. Lower values of aH_2O reduce calculated pressures by around 0·5 kbar at aH_2O = 0·15, a value at the lower end of the range measured by Harley & Carrington (2001). We assume that there is no CO_2 in cordierite, in part because of the general absence of calc-silicate within the SBMB. However, even the addition of significant quantities of CO_2 produces only a small effect on the calculated results, e.g. increasing P by around 0·2 kbar for aCO_2 = 0·4 and aH_2O = 0·4. It is apparent from the ubiquitous marginal replacement of sillimanite by cordierite that the former was not in equilibrium during the final stages of retrograde reaction; consequently, Table 2 includes calculations that omit sillimanite (and spinel) from the stable assemblage. Where present, spinel occurs with sillimanite and in contact with cordierite but is not found in contact with either quartz or garnet, suggesting small domainal

Table 1: Results of THERMOCALC average P–T *calculations using representative garnet core/peak compositions and inclusions of biotite and plagioclase (i.e. inferred peak metamorphic conditions)*

Sample*	Location	Rock type	av*T* (°C)	sd*T*	av*P* (kbar)	sd*P*	cor	sd(fit)	J&B (1990)†	
									T@7 kbar	*P*@700°C
A1	Port Navalo	Metatexite mesosome	889	162	11·5	2·8	0·85	0·1	742–904	8·6–9·0
A2	Port Navalo	Metatexite	782	136	8·7	2·4	0·78	0·9	747–915	5·7–6·5
A3	Port du Crouesty	Grt metatexite	701	120	4·6	2·1	0·61	0·5	667–733	6·9–7·7
A5	Port du Crouesty	Diatexite	790	134	9·6	2·4	0·80	0·7	732–879	7·2–8·0
A6	Port Navalo	Grt–Crd gneiss	857	147	10·7	2·7	0·80	0·2	709–828	7·8–8·1
A7	St. Nazaire	Grt–Crd gneiss	784	138	9·5	2·4	0·82	0·6	714–839	8·3–9·4
A8	Port Navalo	Morbihanite	673	116	4·6	1·8	0·68	0·2	674–748	5·5–6·1
A9‡	Roguedas	Morbihanite	600	—	4·2	1·5	—	1·3	599–626	8·8–9·9
	Roguedas	Morbihanite	800	—	6·2	3·5	—	2·3		
	Roguedas	Morbihanite	1000	—	8·3	5·5	—	3·1		

Data source: Jones & Brown (1990).
*Relevant data table from the appendix of Jones & Brown (1990).
†Results of Jones & Brown (1990) using averaged compositions.
‡Average *P* calculations at fixed *T*.

Table 2: Results of THERMOCALC average P–T *calculations using garnet rim compositions and proximal symplectic biotite, plagioclase ± cordierite, spinel (i.e. inferred retrograde metamorphic conditions)*

Sample*	Location	Rock type	av*T* (°C)	sd*T*	av*P* (kbar)	sd*P*	cor	sd(fit)	J&B (1990)†	
									T@5 kbar	*P*@500°C
A1	Port Navalo	Metatexite mesosome	778	137	6·8	2·2	0·74	0·1	700–794	3·7–4·8
A2	Port Navalo	Metatexite	672	142	3·4	1·4	0·93	1·6	640–672	3·7–4·8
A2‡	Port Navalo	Metatexite	652	187	2·1	3·2	0·61	2·2		
A4	Port Navalo	Diatexite	777	141	8·5	2·4	0·78	0·1	659–706	4·4–5·4
A5	Port du Crouesty	Diatexite	666	78	4·2	0·8	0·88	0·8	632–659	3·7–4·8
A5‡	Port du Crouesty	Diatexite	666	80	4·2	1·5	0·61	0·9		
A5§	Port du Crouesty	Diatexite	737	117	4·2	2·3	0·31	0·2		
A6	Port Navalo	Grt–Crd gneiss	728	91	4·2	0·8	0·91	0·7	622–646	3·3–4·4
A6‡	Port Navalo	Grt–Crd gneiss	730	94	4·2	1·6	0·64	0·8		
A6§	Port Navalo	Grt–Crd gneiss	804	137	4·5	2·5	0·37	0·9		
A7	St. Nazaire	Grt–Crd gneiss	805	140	4·6	1·2	0·91	1·4	707–811	3·9–4·9
A7‡	St. Nazaire	Grt–Crd gneiss	785	149	3·3	2·4	0·60	1·5		
A8	Port Navalo	Morbihanite	670	103	2·6	0·9	0·96	1·1	555–579	2·3–3·5
A8‡	Port Navalo	Morbihanite	670	122	2·5	2·0	0·66	1·2		
A9	Roguedas	Morbihanite	671	169	3·0	1·6	0·96	1·84	600–609	3·3–4·9
	Roguedas	Morbihanite	661	196	2·5	3·3	0·68	2·12		

Data source: Jones & Brown (1990).
*Relevant data table from the appendix of Jones & Brown (1990).
†Results of Jones & Brown (1990) using averaged compositions.
‡Sil and Spl omitted from stable assemblage.
§Spl-bearing domains (i.e. Qtz + Grt omitted).

equilibration volumes; calculations involving spinel omit quartz and garnet (Table 2).

The recalculated results compare well with those of Jones & Brown (1990) and in most cases the error ellipses intersect. Calculated P for A3 (peak; Table 1) and A4 (retrograde; Table 2) are higher than those calculated by Jones & Brown. The omission of sillimanite from the stable retrograde assemblage increases the errors, particularly for P, which is on average approximately 1 kbar higher than for sillimanite-present assemblages (1σ). The average recalculated result suggests peak metamorphic conditions of $P \approx 8{\cdot}5$ kbar, $T \approx 780°C$ (calculated result $8{\cdot}3 \pm 2{\cdot}4$ kbar, $782 \pm 136°C$), and high-T retrograde replacement of garnet at $P \approx 4{\cdot}5$ kbar, $T \approx 780°C$ ($4{\cdot}7 \pm 1{\cdot}7$ kbar, $780 \pm 131°C$).

MnNCKFMASH PHASE EQUILIBRIA

Subsolidus and suprasolidus metapelitic phase relations were modelled in the MnNCKFMASH system using THERMOCALC v. 3.1 (Powell & Holland, 1988) and the dataset of Holland & Powell (1998; updated 14 May 2001). Calculations consider the following phases: garnet; chlorite; staurolite; biotite; cordierite; orthopyroxene; muscovite; paragonite; zoisite; plagioclase; K-feldspar; quartz; H_2O; melt (L). Although paragonite, zoisite and orthopyroxene have not been identified, these phases provide critical constraints on the stability of phases that are present, particularly staurolite. Mixing models follow Holland & Powell (2001; NCKASH), White *et al.* (2001; NCKFMASH) and Tinkham *et al.* (2001; MnNCKFMASH) (see Johnson *et al.*, 2003*a*). Following the arguments of Johnson *et al.* (2003*a*), we have modified the Holland & Powell (1998; updated 14 May 2001) data by increasing the enthalpy of formation (ΔH_f) of sillimanite by 0·25 kJ/mol, within the quoted 1σ error of 0·7 kJ/mol. The triple point calculated using the modified data, at $4{\cdot}42 \pm 0{\cdot}1$ kbar, $554 \pm 8°C$, is within error of that favoured by Pattison (1992), and allows a more realistic stability field for andalusite (with staurolite), consistent with natural assemblage data (e.g. Pattison, 1992; Cesare *et al.*, 2003).

Protolith compositions for the migmatites of the SBMB are poorly constrained. It is not possible to trace the migmatites into unmigmatized equivalents, as boundaries to the SBMB are tectonic (Fig. 1). The migmatites themselves are residual, being depleted with respect to a granitic component, although abundant cumulate leucosome (around 50 vol. %; Marchildon & Brown, 2003) implies a large melt flux through the structural level now exposed. Thus, using bulk compositions of rocks from the SBMB is inappropriate.

In this analysis, we have constructed pseudosections based on an average subaluminous metapelitic composition, the mean of 554 analyses taken from the literature [Shaw, 1956 ($n = 155$); Senior & Leake, 1978 ($n = 120$); Atherton & Brotherton, 1982 ($n = 230$); Dalrymple, 1995 ($n = 15$); Solar & Brown, 2001 ($n = 13$); Tinkham, 2002 ($n = 21$); Table 3]. A subaluminous metapelite protolith is implied for most rocks of the SBMB, based on the abundance of biotite and scarcity of sillimanite in rocks other than morbihanite. Although composition is potentially problematic, it is likely that the overall topology of the pseudosections is correct; small bulk compositional variations may affect the absolute position in P–T space of mineral assemblage boundaries and the relative abundance of phases.

Table 3: Major oxide analysis of the average subaluminous metapelite

	wt %	mol %
SiO_2 (S)	59·49	69·75
TiO_2	1·01	
Al_2O_3 (A)	18·70	12·92
FeO* (F)	7·31	6·27
MnO (Mn)	0·14	0·14
MgO (M)	2·61	4·57
CaO (C)	1·36	1·48
Na_2O (N)	1·96	2·23
K_2O (K)	3·52	2·64
P_2O_5	0·14	
LOI	3·32	
Total	99·56	100·00

Mol % values are normalized MnNCKFMAS (anhydrous) and take account of FeO ($=TiO_2$ in ilmenite and CaO ($=3{\cdot}33P_2O_5$) in apatite.
*All Fe as FeO.

Figure 5 shows a P–T pseudosection for the average subaluminous metapelite that illustrates subsolidus and suprasolidus stable parageneses; subsequent phase diagrams are based on this primary pseudosection. Subsolidus assemblages are considered to have equilibrated with a pure H_2O volatile phase. Whereas the presence of graphite (Fig. 2a) will reduce aH_2O via the incorporation of additional species (CO_2, CH_4) into the volatile phase, such buffering effects are small at the P–T conditions of interest (molar $X_{H_2O} > 0{\cdot}85$, $X_{CO_2} < 0{\cdot}08$; Connolly & Cesare, 1993). Subsolidus field boundaries shift to slightly lower T (<10°C); solidus temperatures are similarly raised.

In calculating suprasolidus phase relations, the bulk composition was adjusted to contain just enough H_2O to saturate the solidus at $P = 10$ kbar; consequently, predicted mol % melt at lower P is artificially high. This

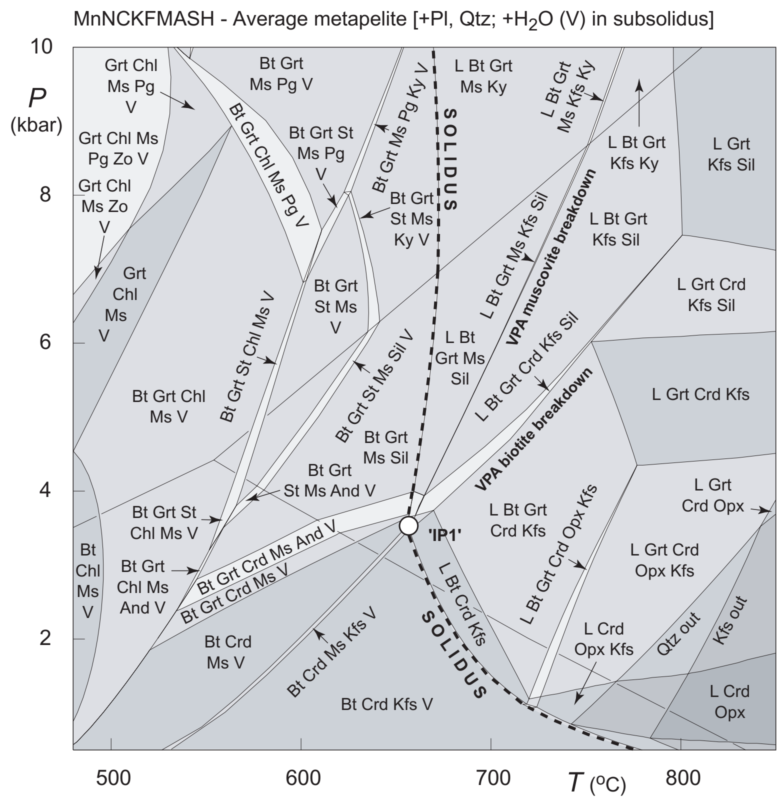

Fig. 5. MnNCKFMASH P–T pseudosection for an average subaluminous metapelite showing calculated stable parageneses. This phase diagram forms the basis for subsequent pseudosections. The depth of shading reflects increased variance; the darkest field (bottom right) is septivariant (F = 7). Mineral abbreviations follow Kretz (1983).

effect becomes pronounced only in rocks that followed a prograde P–T trajectory that crossed the solidus below the low-variance point 'IP1' (Fig. 5), but has little effect on predicted melt production for rocks of this study; excess melt fractions are <1 mol % at $P_{\text{solidus}} > 7$ kbar (see Fig. 7). The suprasolidus part of Fig. 5 shows the position of the important volatile phase-absent (VPA) melting reactions consuming muscovite and biotite + sillimanite, which are narrow trivariant fields in the MnNCKF-MASH system. In Fig. 5, no solid phases were assumed to be in excess, although quartz and plagioclase are predicted in all assemblages within the P–T window of interest and are omitted from the labelled multivariant fields for clarity. In THERMOCALC, molar proportions of all phases are recalculated on a one-oxygen basis; consequently, mol % generally can be considered to approximate vol %.

Additional components

Before discussing phase equilibria, it is important to consider the effect of additional components, particularly Ti and Fe^{3+}. Ti is present (in more than trace amounts) only in ilmenite, rutile and biotite. Whereas ilmenite and rutile are potentially useful in constraining P, their stability is strongly dependent on the abundance of free O_2 (i.e. Fe_2O_3; White *et al.*, 2000). The occurrence of staurolite and garnet in metapelitic rocks during the prograde evolution suggests that the rocks were only weakly oxidized (White *et al.*, 2000).

In the MnNCKFMASHT system, pseudosections calculated to include Ti with no excess O_2 (Zeh & Holness, 2003) predict an unrealistically large stability field for paragonite at low P (<4 kbar) and phase relations between kyanite, staurolite, ilmenite and rutile that are irreconcilable with any reasonable prograde P–T evolution (from our calculations, the inferred sequence kyanite + ilmenite → staurolite + rutile requires increasing P and falling T along the 'prograde' path for a fixed quantity of O_2). These problems may reflect changing oxidation states during metamorphism or problems with the activity model for paragonite and/or biotite. The predicted stability field of paragonite in the MnNCKFMASH system, at $P > 7$ kbar, is consistent with the presence of sodic white mica in metapelitic rocks metamorphosed under moderate- to high-pressure conditions.

The principal qualitative effect of Ti on the pseudosections will be to increase the upper T stability of biotite; the

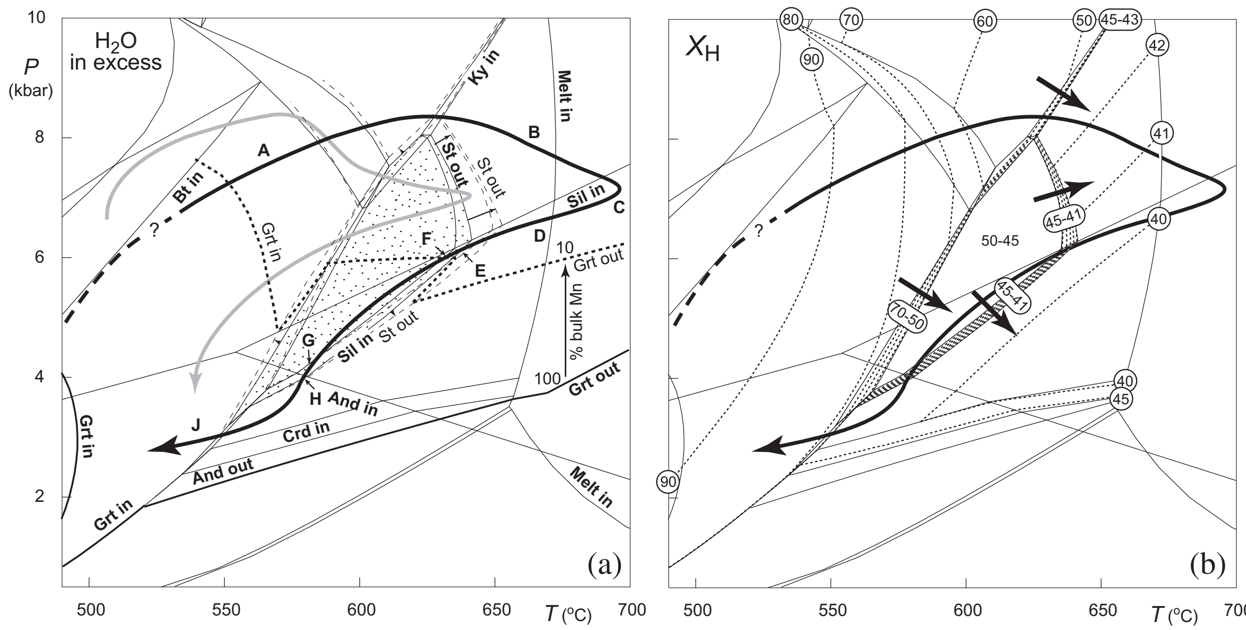

Fig. 6. MnNCKFMASH P–T pseudosections illustrating subsolidus phase equilibria (see text for detailed discussion). (a) The simplest P–T path consistent with the observed phase equilibria and thermobarometric estimates is shown by the bold black curve. The stippled field shows staurolite stability, which is expanded by subtraction of Mn. The grey P–T path is that invoked by Triboulet & Audren (1985). (b) Subsolidus field contoured for X_H, the quantity of H_2O required to saturate the assemblage at specified P–T as a percentage of that required to saturate the most H_2O-rich (chlorite-bearing) assemblage, which occurs in the top left corner.

points (at which four fields intersect) within the suprasolidus region of the MnNCKFMASH pseudosections that involve the disappearance of biotite will migrate along the appropriate biotite-out field boundary to higher T. The presence of Zn will expand the stability field of staurolite. Staurolite inclusions within garnet contain about 0·5 wt % Zn (Jones & Brown, 1990), and the effect of Zn is probably small (e.g. Pattison *et al.*, 1999). The staurolite field will also be expanded in more Fe-rich protolith compositions (see Johnson *et al.*, 2003*a*).

Subsolidus phase equilibria

Figure 6a illustrates the lower-T phase equilibria and is appropriate for discussion of the metapelites along the Vilaine estuary (Fig. 1). The P–T path proposed by Triboulet & Audren (1985) is superimposed on Fig. 6a (pale grey), together with a P–T path that is consistent with phase equilibria (black) as discussed below. On the basis of microstructural observations and/or chemographic relations in the simplified KFMASH model system, Triboulet & Audren suggested the following sequence for the onset of growth of important phases in the metapelites. Along the prograde P–T path, kyanite was followed by sillimanite and biotite, and along the retrograde P–T path, sillimanite and biotite were followed by staurolite and garnet, and then andalusite (replacing staurolite), with continuous growth of biotite, garnet and staurolite up to the onset of andalusite development. Staurolite growth continued beyond that of garnet. Sillimanite growth is inferred to have occurred in two stages, with late-stage development followed closely by the growth of andalusite (Triboulet & Audren, 1985, Table 1).

A critical consideration in the development of subsolidus prograde and retrograde assemblages is the behaviour and availability of H_2O (see Guiraud *et al.*, 2001). Figure 6b shows the subsolidus field contoured for the quantity of H_2O (X_H) required to just saturate the rock as a percentage of that required to saturate the most H_2O-rich (chlorite-rich) assemblage. In the absence of an external supply of H_2O, and assuming H_2O produced by dehydration reactions is lost from the equilibration volume, reaction will occur only along segments of the P–T path towards lower values of X_H (Guiraud *et al.*, 2001). The highest reaction rates for a fixed rate of change of P–T occur across the lowest variance (trivariant) fields (arrows in Fig. 6b).

Prograde evolution

An important initial consideration is the prograde behaviour of garnet. For the average metapelite composition, prograde garnet growth (e.g. along segment A) is predicted to begin at $T < 500°C$. At low T, garnet is stabilized by Mn, as evidenced by the near ubiquity of spessartine-rich cores in subsolidus garnet that preserves growth zoning (e.g. Tracy *et al.*, 1976; Mahar *et al.*, 1997; Tinkham *et al.*, 2001). In spite of modification of garnet zoning profiles by retrograde diffusion (Fig. 4a), garnet from metapelites in the Vilaine estuary is Mn-rich (X_{Sps} up to 0·13 in staurolite layers and 0·25 in staurolite-absent layers). Although the Mn content of the protolith is not known, the bold dashed line in Fig. 6a shows the effect of reducing the bulk Mn in the average metapelite to 10% of the total (i.e. 0·014 mol %). At the inferred *P* of prograde metamorphism, the onset of garnet growth is predicted at $T \approx 550°C$ even in Mn-depleted rocks, some 100°C before kyanite development (Fig. 6a). On the basis of KFMASH chemographic relations, Triboulet & Audren (1985) suggested that the onset of garnet growth occurred after that of kyanite during retrograde metamorphism. Such a conclusion is inconsistent with the phase equilibria in the enlarged system and the zonal sequence of index minerals in moderate-*P* (Barrovian) regional metamorphic terranes worldwide.

Growth of kyanite (along segment B) before staurolite requires a prograde *P–T* path at pressures above that of the staurolite stability field (stippled field in Fig. 6a), i.e. $P > 8$ kbar. Sillimanite growth at the metamorphic peak (point C) obviously requires higher *T*. Although a *P* decrease is not necessarily required, isobaric heating at $P > 8$ kbar would result in sillimanite growth at or beyond the suprasolidus VPA breakdown ('dehydration' melting) of muscovite (Fig. 5). In such circumstances, the rocks would be expected to show evidence for moderate degrees of partial melting (around 10 vol. %) and there would be an absence of primary (fabric-forming) muscovite. As such features are not observed, it is likely that the attainment of peak metamorphic conditions involved some decompression (around 2 kbar) following kyanite development, consistent with a clockwise *P–T* evolution. The simplest *P–T* trajectory suggests that sillimanite growth occurred within the suprasolidus field but before the onset of major volatile phase-absent melting (Figs 5 and 6a). In these circumstances, predicted melt fractions of 1–2 vol. % might be difficult to identify in regionally metamorphosed rocks that have undergone subsequent deformation and retrograde reaction.

Figure 6b implies that continuous, close to closed-system reaction (i.e. excluding loss of liberated volatile phase at subsolidus conditions) will occur along the prograde path up to the metamorphic peak. Assuming the small volumes of melt generated at the metamorphic peak are retained within the equilibration volume, the value of X_H is likely to correspond to the value as the solidus is crossed (i.e. $X_H \approx 40$ for the preferred *P–T* path; Fig. 6b).

Retrograde evolution

In the early stage of the retrograde evolution, growth of staurolite (with biotite) and consumption of sillimanite is inferred. Later retrograde reaction resulted in a second stage of sillimanite growth, and consumption of garnet followed by staurolite, with andalusite replacing staurolite (Fig. 2a). A final stage in the retrograde evolution resulted in replacement of andalusite by white mica (Fig. 2b; Triboulet & Audren, 1985). This sequence provides important constraints on conditions during the retrograde segment of the *P–T* path.

Cooling with continued decompression from the metamorphic peak potentially results in minor sillimanite and garnet resorption (Fig. 6a, segment D). Importantly, retrograde staurolite growth (at E) followed by sillimanite consumption (at F) is predicted only if an external supply of H_2O is available, as this segment of the retrograde path is characterized by increasing X_H (Fig. 6b) and a value of X_H at the initiation of the reaction that is slightly greater than that at the metamorphic peak. A second phase of sillimanite growth (at G) is synchronous with the onset of staurolite resorption, a reaction characterized by decreasing X_H. Whereas the minimum quantity of H_2O necessary for retrograde sillimanite and staurolite growth ($X_H = 41$) is marginally higher than that inferred at the metamorphic peak ($X_H \approx 40$), the errors on the X_H isopleths, although difficult to quantify, allow that an external supply of H_2O may not be necessary to initiate reaction. However, the size of partially pseudomorphed staurolite crystals within appropriate layers (e.g. Fig. 2a and b) indicates that H_2O-rich volatile-phase influx probably did occur. The replacement of staurolite by andalusite (at H) is constrained to occur at $P \approx 4$ kbar, $T \approx 600$–550°C and requires higher decompression rates. Continued cooling allows andalusite to be replaced by white mica (at J), but only if an H_2O-rich volatile phase is supplied from an external source (Fig. 6b). The absence of cordierite suggests that the retrograde *P–T* path passed close to $P \approx 3$ kbar, $T \approx 550°C$.

Prograde garnet growth and sequestering of Mn into this phase results in the effective bulk composition (Stüwe, 1997; Marmo *et al.*, 2002) becoming depleted in Mn; garnet growth along the retrograde path is inhibited and garnet stability is shifted to higher *P*. An important consequence is that the staurolite stability field is enlarged, by up to around 0·5 kbar, 25°C at its high *P–T* termination (Fig. 5a). At low *P*, where garnet abundances are low regardless of Mn content, this effect is negligible. Increased Fe and Al in the protolith will enlarge the staurolite stability field at all pressures (e.g. Johnson *et al.*, 2003*a*).

Suprasolidus phase equilibria

Figure 7 illustrates the higher-*T* phase equilibria appropriate for the discussion of the migmatitic rocks occurring within the SBMB. Garnet cores within migmatites exhibit modified growth zoning with flattened bell-shaped Mn

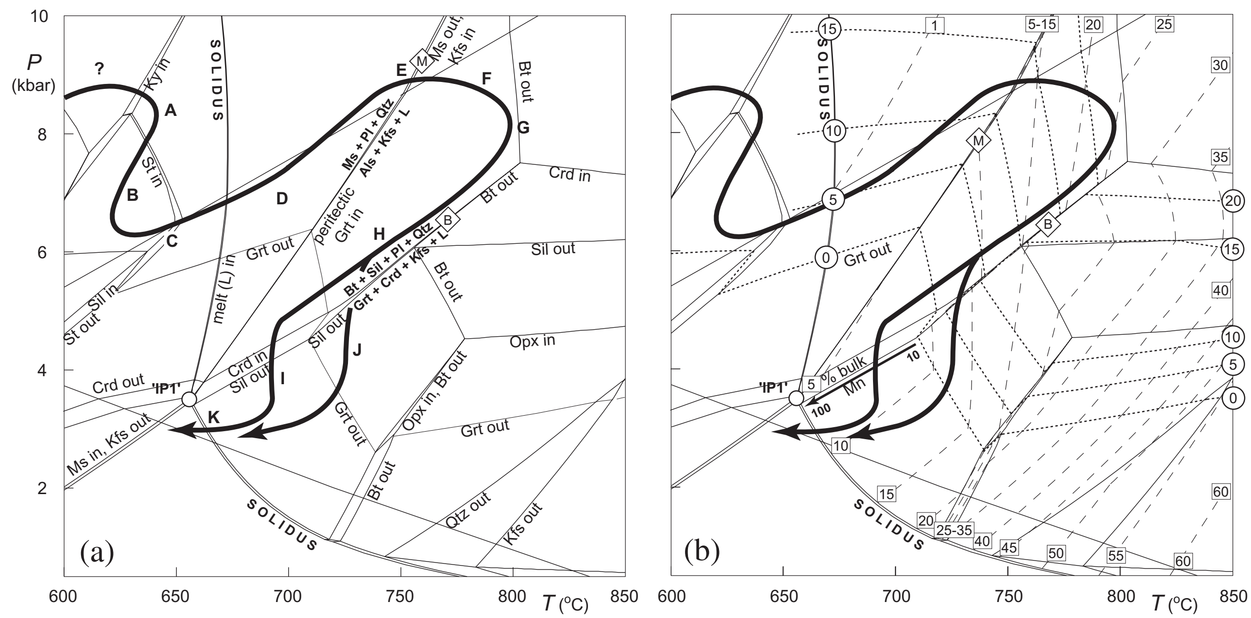

Fig. 7. MnNCKFMASH P–T pseudosections illustrating suprasolidus phase equilibria for an average metapelite with 10% of bulk Mn (see text for detailed discussion). An example P–T path that is consistent with petrographic and thermobarometric constraints is shown by the bold black curve. (a) Stable assemblages illustrating the appearance or disappearance of phases. (b) Contoured proportions (as mol %) of melt (fine dashed lines) and garnet (fine dotted lines) in the suprasolidus field. Reactions M and B are the major volatile phase-absent melting reactions consuming muscovite and biotite + sillimanite, respectively.

profiles (Jones & Brown, 1990; Fig. 4b and c), suggesting Raleigh fractionation of Mn and its removal from the effective bulk composition. For this reason, Fig. 7 is constructed for the average subaluminous metapelite with 10% of the bulk Mn content. Consequently, the predicted molar proportions of garnet do not take into account spessartine-rich cores that grew at low T, essentially showing only the quantity of post-kyanite garnet production.

Sequential zones of inclusion suites within garnet and reaction microstructures provide critical constraints on the P–T path for the SBMB (Fig. 3b). The petrographic relations suggest that the onset of prograde growth of important phases was garnet followed by kyanite (as inclusions in inner cores), staurolite (with kyanite or sillimanite as inclusions in outer cores) and sillimanite (inclusions in outer cores); kyanite occurs as inclusions within leucosome plagioclase, suggesting that it was in equilibrium with melt and the peritectic growth of garnet and sillimanite occurred as melt fraction increased with rising temperature. The implied retrograde reaction sequence was sillimanite and biotite (replacing garnet; Fig. 3a and c) followed by cordierite with or without spinel (replacing polymineralic aggregates; Fig. 3c–e) and peritectic cordierite in association with a second phase of melt production (Fig. 3f). Retrograde reaction is inferred to have occurred where melt remained within the system (Brown & Dallmeyer, 1996). An example of a P–T path consistent with the petrographic constraints is superimposed on Fig. 7 and discussed below.

Prograde evolution

The inclusion of kyanite and the absence of staurolite within the innermost garnet cores (Fig. 3b) is consistent with the early subsolidus segment of the prograde P–T path having passed above the staurolite stability field, implying $P > 8$ kbar, $T \approx 640$°C (Fig. 7, segment A). Growth of staurolite with either kyanite or sillimanite, which occur as inclusions in the inner and outer core regions of garnet, respectively, requires decompression, with or without cooling (segment B) followed by heating close to the intersection of the aluminosilicate + staurolite field with the kyanite–sillimanite transition (point C), implying conditions of $P \approx 6{\cdot}5$ kbar, $T \approx 650$°C, consistent with calculations based on GRAIL (Jones & Brown, 1990). Segment B of the P–T path into the staurolite field is associated with an increase in X_H (Fig. 6b); in the absence of an external source of H_2O, no reaction will occur. However, growth of kyanite or sillimanite and some staurolite will occur along the prograde segment and within the narrow trivariant field around point C, without the addition of any externally derived H_2O (Fig. 6b), consistent with the small quantities of staurolite present.

The presence of sillimanite without staurolite in the outer cores of garnet implies sillimanite stability and continued garnet growth following staurolite consumption (along segment D). The presence of kyanite relics in leucosome plagioclase implies that kyanite was the stable Al_2SiO_5 polymorph at the onset of major melting by VPA muscovite breakdown (point E); conditions of $P > 9$ kbar, $T \approx 750°C$ are implied.

Along the P–T path, up to 5 mol % melt production is predicted up to the onset of VPA melting consuming muscovite (segment D), where a major melting step occurs (at E, reaction M). Muscovite breakdown results in the production of an additional 10 mol % melt over a small T interval of about 1°C and the consumption of this phase, consistent with the lack of primary muscovite in the migmatites. Kyanite and K-feldspar are products of muscovite breakdown. Kyanite occurs within magmatic plagioclase within the leucosome; K-feldspar is rarely present although its former presence can be inferred by the occurrence of myrmekite and/or quartz–muscovite intergrowths (Jones & Brown, 1990). The prograde evolution to the metamorphic peak (along segment F) is marked by the kyanite–sillimanite transition and results in melt fractions increasing to around 25 mol % (Fig. 7b) via the breakdown of biotite + kyanite/sillimanite (+ plagioclase, quartz) to garnet + melt (+K-feldspar). The proportion of garnet increases by about 15 mol % as a result of peritectic garnet growth (Fig. 7b). Peritectic garnet growth may have occurred as inclusion-poor overgrowths on pre-existing grains or as new grains associated with leucosome. The metamorphic peak (point G) corresponds to that inferred by Jones & Brown (1990), consistent with the recalculated results presented in Table 1. There is no evidence for cordierite growth at the peak of metamorphism, implying that the P–T path did not cross the major VPA biotite + sillimanite-consuming melting reaction B. Around 25 mol % melt is predicted at the metamorphic peak, but melt loss from these rocks is likely to have occurred; this implies a flux of melt through these rocks around metamorphic peak conditions.

Retrograde evolution

The early stage of retrograde reaction during conductive cooling is recorded by the marginal replacement of garnet, principally by biotite (and plagioclase, with or without sillimanite) consistent with reaction between garnet and melt on cooling (Fig. 7b). A primary constraint on the early retrograde path is the narrow trivariant field that records major biotite + sillimanite breakdown (Fig. 7, reaction B). Crossing this reaction along the retrograde path requires a reduction in P and results in melting and the production of both peritectic cordierite and garnet, and the resorption of both biotite and sillimanite; biotite is consumed at high P/T and sillimanite at low P/T (Fig. 7a). Both biotite and, less commonly, sillimanite are products of early retrograde reaction, not reactants, indicating that the early retrograde path passed to the high-P, low-T side of the trivariant field representing reaction B (along segment H). The general lack of retrograde muscovite and abundance of sillimanite implies the early retrograde path remained to the low-P, high-T side of the major muscovite-consuming reaction (reaction M).

The later stage of retrograde reaction, in which garnet, biotite, sillimanite and plagioclase are replaced by cordierite, involves a second episode of melt production and growth of peritectic cordierite. This implies a segment of the retrograde P–T path with a steeper dP/dT than the early stage. The ubiquitous mantling of sillimanite by cordierite suggests that it was not part of the stable assemblage, consistent with segment I (Fig. 7a). Isothermal (at 700°C) decompression along segment I results in a small amount of melting (up to 5 mol %) and production of >25 mol % peritectic cordierite (Fig. 7). Whereas segment I is shown as near isothermal decompression from $P \approx 5$ kbar to 3 kbar, the data do not preclude some additional heating that will increase melt fractions by a few mol %. Increasing the bulk Mn of the protolith results in the major garnet + cordierite + melt-producing trivariant field (reaction B) extending to lower P–T (Fig. 7b) and will produce a small quantity of garnet (1–2 mol %) in addition. Decompression at higher T (segment J) produces a larger volume (around 5 mol %) of additional peritectic garnet. The presence of garnet in most rocks, even as highly resorbed grains, suggests stabilization by Mn and/or sluggish reaction and/or melt loss (e.g. Powell & Downes, 1990; Brown, 2002; White & Powell, 2002; Johnson *et al.*, 2003*b*).

Following decompression melting, subsequent rapid, near-isobaric cooling (Brown & Dallmeyer, 1996; segment K) results in the P–T path crossing the solidus below the low-variance point 'IP1' at about 660°C, at which point extensive retrograde reaction is likely to have stopped. This T is at the lowermost end of the average calculations shown in Table 2. An important consequence is that the final stage of suprasolidus and high-T subsolidus reaction does not produce muscovite (Spear *et al.*, 1999), consistent with the scarcity of retrograde muscovite within the SBMB.

The effect of melt loss

Whereas the phase relations shown in Fig. 7 are broadly consistent with petrographic observations, the presence of residual peritectic garnet in most rocks suggests that the migmatites are melt depleted, even though they contain about 50 vol. % leucosome (Marchildon & Brown, 2003). At first sight this seems to represent a paradox. However, most of the leucosome appears to be cumulate in composition, which suggests that melt was fluxed through these rocks from deeper levels in the crust, but was fractionated by partial crystallization in the ascent

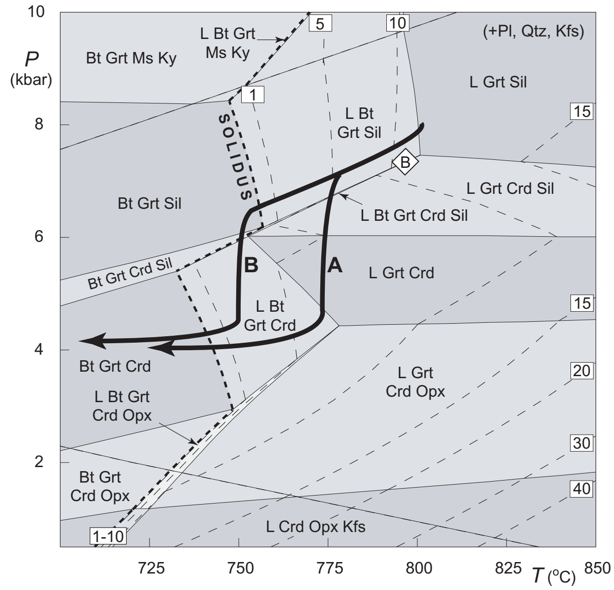

Fig. 8. MnNCKFMASH P–T pseudosection illustrating the effect of 60% melt loss at the metamorphic peak (i.e. reducing the melt fraction from 25 to 10 mol %). This diagram is appropriate only for the consideration of retrograde phase equilibria. The principal effect of melt (and H_2O) loss is the elevation of solidus temperatures and an increased stability of garnet. Two alternate P–T paths consistent with petrological and thermobarometric constraints are shown by bold black curves; these are discussed further in the text. The darkest fields are quinivariant (F = 5).

channels. As melt flux declined during cooling and crystallization along the retrograde P–T path, minimal derived melt was retained at the structural level now exposed, allowing preservation of residual peritectic garnet. The second episode of melting led to the development of peritectic cordierite and leucosome in interboudin partitions, consistent with a second episode of melt flux through these rocks to feed granite plutons at higher crustal levels (Marchildon & Brown, 2003). Again, minimal derived melt was retained at the structural level now exposed, allowing preservation of residual peritectic cordierite.

Figure 8 shows phase equilibria for a rock that attained peak metamorphic conditions and lost 60% of the 25 mol % melt predicted (i.e. retention of the net equivalent of 10 mol % melt) and is only appropriate for examination of phase equilibria along the retrograde path. The two principal effects of the bulk compositional change following melt loss (and the consequent loss of most of the H_2O) are that the solidus becomes stepped and is raised to higher T, and that garnet is stable in all but the lowest-P paragenesis. The loss of sillimanite from the stable assemblage implies decompression and crossing of the narrow trivariant field that defines reaction B. Reaction across this field results in sillimanite and biotite resorption and produces a small quantity of garnet (2–3 mol %) and melt (3 mol %) with a large amount of cordierite (14 mol %). Whereas biotite consumption is predicted in MnNCKFMASH, Ti will stabilize this phase to higher T. Continued near-isothermal decompression results in garnet resorption but continued production of cordierite (with biotite). A temperature rise may have accompanied the decompression segment, resulting in increased melt production, but this is beyond the resolution of our analysis.

The T at which the decompression segment occurs is potentially important. At higher T (path B), some melt will be present throughout (Fig. 8). At lower T (<750°C, path A), the rocks are predicted to be subsolidus at the initiation of the steep decompression segment. Near-isobaric cooling at 4 kbar results in crystallization of melt at about 740°C, at which point extensive retrograde reaction is likely to have stopped. Such temperatures are more consistent with thermobarometric estimates of conditions during retrograde evolution (Table 2).

DISCUSSION

MnNCKFMASH phase equilibria

Subsolidus

Given the thermobarometric and microstructural constraints, Fig. 6 adequately describes the P–T evolution of subsolidus metapelitic rocks exposed in the Vilaine estuary. The P–T path that most simply satisfies the petrological constraints has a similar geometry to that proposed by Triboulet & Audren (1985); predicted pressures show excellent agreement, but the predicted temperatures are around 50°C higher than those proposed by those workers, which were based on Fe–Mg exchange thermometry. This discrepancy is consistent with retrograde Fe–Mg exchange (e.g. Pattison *et al.*, 2003). The prograde growth sequence garnet → kyanite → sillimanite is consistent with continuous dehydration reactions along a prograde clockwise P–T segment with a peak $P \geq$ 8 kbar at T = 625–650°C, and peak metamorphic conditions of P = 6–7 kbar, T = 650–700°C.

Figure 6b suggests that retrograde development of abundant staurolite and sillimanite, the subsequent replacement of staurolite by andalusite and localized replacement of andalusite by white mica required an external supply of H_2O. The rocks in the Vilaine estuary were underlain by melt-bearing rocks of the SBMB and the contact between the Vilaine Group and the SBMB contains granite that is coeval with the decompression segment of the P–T path (Bernard-Griffiths *et al.*, 1985; Brown & Dallmeyer, 1996). As the migmatites are inferred to record net melt loss from both episodes of melting, it is unlikely that during final crystallization much H_2O-rich volatile phase was released from these rocks. However, as the granite cooled, crystallizing melt is likely to have released an H_2O-rich volatile phase into overlying rocks, driving the observed retrograde reaction sequence during decompressive cooling.

Suprasolidus

Suprasolidus phase relations allow construction of a P–T path for the migmatites that is consistent with thermobarometric and microstructural constraints and previously invoked P–T paths. The subsolidus prograde path is similar to that implied for the rocks in the Vilaine estuary, with development of garnet and kyanite, followed by a decompression segment then further heating, during which staurolite and kyanite or sillimanite grew; no addition of H_2O is required. At the metamorphic peak, total melt production was about 25 mol %. Whereas the retrograde evolution of the migmatites potentially can be explained without invoking melt loss (Fig. 7), calculated temperatures of retrograde re-equilibration, which are likely to record crossing of the solidus, are more consistent with phase equilibria for melt-depleted bulk compositions (Fig. 8), consistent with net melt loss.

Temperatures recalculated for both peak and retrograde conditions are statistically identical (around 780 ± 130°C; Tables 1 and 2). These results are consistent with isothermal decompression close to the metamorphic peak, as inferred by Jones & Brown (1990). However, reaction microstructures involving partial replacement of garnet can be reconciled with phase equilibria only if a segment of post-peak conductive cooling preceded the steep decompression segment, implying exhumation and subsequent rapid cooling, consistent with the interpretation of Brown & Dallmeyer (1996).

Garnet growth and compositional zonation

Figure 9 shows the predicted molar quantities of garnet for the average subaluminous metapelite and compositional isopleths (as percent mole fraction; i.e. $100X_{Py}$, etc.) of pyrope, grossular and spessartine components. X_{Alm} (not shown) essentially varies antithetically with X_{Py}. We use Fig. 9 to interpret the garnet maps and quantitative analyses as shown in Fig. 4. Whereas small bulk compositional variations will affect the modal abundance of garnet, the geometry of the isopleths is not significantly altered.

Subsolidus garnet growth—Vilaine metapelite

Along the subsolidus prograde path inferred for metapelitic rocks of the Vilaine estuary, the bulk of garnet growth occurs at low T, until the onset of kyanite growth, where 10–15 mol % garnet is predicted. Along the proposed prograde path, X_{Py} increases and both X_{Gr} and X_{Sps} decrease. At the inferred metamorphic peak X_{Py}, X_{Gr} and X_{Sps} have predicted values of around 0·18, 0·04 and 0·04, respectively. Although caution should be applied to equilibrium interpretations of Ca distribution in garnet (Chernoff & Carlson, 1997), variations in X_{Gr} (Fig. 4a) suggest preservation of growth zoning, consistent with the slow diffusivity of Ca in garnet (e.g. Carlson, 2002). However, the decrease in Mg and increase in Mn from core to rim (Fig. 4a) suggest homogenization at the peak of metamorphism followed by retrograde diffusion, implying diffusive length scales for these cations at the metamorphic peak that exceeded the grain size of this garnet (around 0·5 mm).

Measured concentrations of X_{Py} and X_{Sps} (and X_{Alm}) are consistent with garnet cores equilibrating along the retrograde path at conditions close to the replacement of staurolite by andalusite ($P \approx$ 4–5 kbar, $T \approx$ 575°C). Rim compositions for these components suggest equilibration at $P \approx$ 3 kbar, $T \approx$ 525°C. Measured values of X_{Gr} are consistent with core compositions closing to Ca at the pressure peak ($P \approx$ 8 kbar, $T \approx$ 600–625°C), where the abundance of garnet was highest. The X_{Gr} zoning profile is consistent with re-equilibration along the retrograde path, with rims recording conditions close to the retrograde development of andalusite.

Suprasolidus garnet growth—garnet–cordierite gneiss

Garnet growth in the migmatites is predicted to have been a two-stage process (Fig. 9). Most subsolidus growth occurred along the low-T (pre-kyanite) segment of the prograde path, as discussed above. Extensive garnet resorption along the implied subsolidus decompression segment is predicted only if an external supply of H_2O is available (Fig. 6b). A second peritectic growth stage is predicted following volatile phase-absent, muscovite-consuming melting, where garnet contents increase to around 20 mol %. At the inferred metamorphic peak, X_{Py}, X_{Gr} and X_{Sps} are predicted to have values of around 0·35, 0·03–0·04 and 0·01, respectively.

The inclusion-rich core of the analysed garnet from the garnet–cordierite gneiss (Fig. 4b), interpreted to record prograde subsolidus development, preserves evidence for growth zoning, with an increase in Mg and a decrease in Mn (and Fe) from core to rim; although quantitative variations in Mg are small, those in Mn are an order of magnitude different. The extreme edge of the garnet shows a pronounced decrease in Mg and an increase in Mn and Fe, consistent with diffusive retrograde reaction over length scales of 0·1–0·2 mm. Measured values of X_{Py} (and X_{Alm}), which show little variation except at the extreme rims of garnet, are consistent with conditions of $P \approx$ 5–6 kbar, $T \approx$ 750°C, close to the implied conditions during the retrograde segment where the VPA

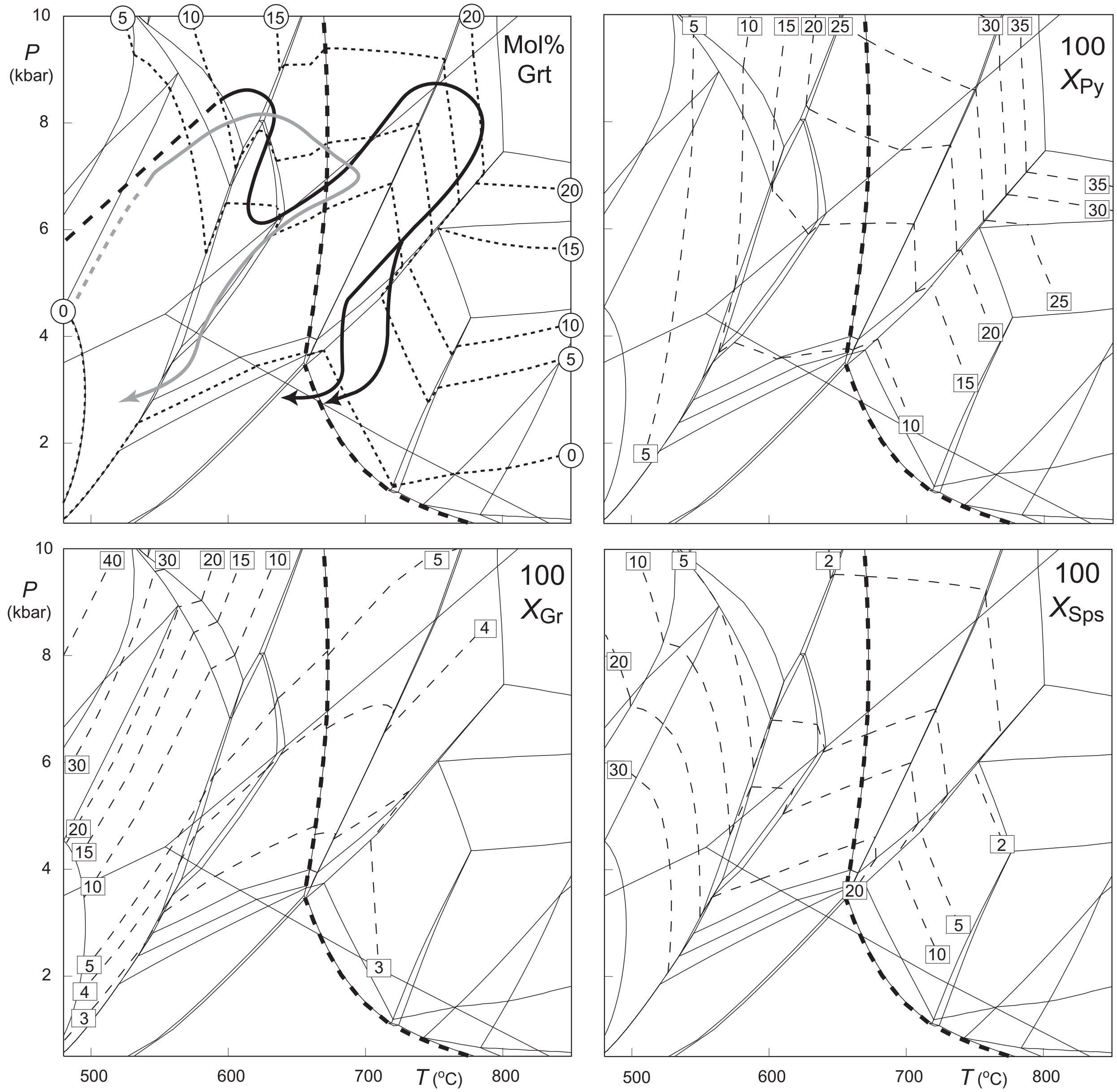

Fig. 9. MnNCKFMASH P–T pseudosections for the average subaluminous metapelite contoured for mol % garnet (example P–T paths from Figs 6 and 7 are shown for reference), and compositional isopleths for the pyrope, grossular and spessartine components.

melting reaction consuming biotite is crossed. Such values are intermediate between those predicted at the metamorphic peak and those as the solidus was crossed, particularly when raised solidus temperatures caused by melt loss are considered (Fig. 8). Given the zoning profile (Fig. 4b map), measured concentrations of Mn in garnet cores correspond well to those predicted at the pressure peak ($P \approx 8{\cdot}5$ kbar, $T \approx 750$°C). The lowest concentrations of Mn, close to the transition between the outer core and the inclusion-poor rim, are consistent with equilibration at the temperature peak ($P \approx 8$ kbar, $T \approx 800$°C), where the abundance of garnet was greatest. The broad inclusion-poor rim, interpreted to represent peritectic garnet growth, exhibits slightly higher values, consistent with some retrograde diffusion down to $T \approx 750$°C. The extreme edge of garnet grains suggests limited diffusion of Mn at temperatures close to and below the solidus.

Although Fe, Mg and Mn distributions are consistent with equilibrium processes, the measured concentration of X_{Gr} cannot be reconciled with Fig. 9, implying grain-scale (around 10 mm) disequilibrium. A zone of increased Ca is apparent that roughly, although not exactly, corresponds to the outer core as defined by the Mg and Mn profiles (Fig. 4b), in which Ca contents are predicted to be lowest. The Ca zoning profile in the garnet–cordierite gneiss is similar to that documented by Spear & Daniel (2001), who noted the incompatibility of predicted equilibrium concentrations with zoning profiles. Those workers suggested that, during growth, the supply of Ca is controlled by diffusive transport between garnet and the immediately surrounding matrix, principally the anorthite component in plagioclase. Their model predicts Ca depletion in the core during growth, consistent with our observations (Fig. 4b; compare fig. 16c of Spear & Daniel, 2001). Disequilibrium for Ca during garnet growth has been demonstrated elsewhere and is probably governed by kinetic factors, principally diffusion rates that are slower than those of Fe, Mg and Mn (e.g. Chernoff & Carlson, 1997; Spear & Daniel, 2001; Carlson, 2002).

Suprasolidus garnet growth—morbihanite

Garnet growth in the morbihanite is likely to have been similar to that in the garnet–cordierite gneiss. The inflection in the zoning profiles is consistent with two stages of growth, similar to the garnet from the garnet–cordierite gneiss. The flattened bell-shaped Mn profile is consistent with preserved growth zoning. However, discounting retrograde reaction around biotite inclusions, the observed smooth decrease in Mg and increase in Fe from core to rim is consistent with homogenization of these cations at the metamorphic peak, followed by retrograde diffusion. Such profiles reaffirm the relative rapidity of Fe and Mg diffusion compared with that of Mn over the length scale of the analysed garnet (2 mm). Ca contents are essentially constant throughout, suggesting grain-scale (around 2 mm) equilibration at the metamorphic peak.

The concentrations of X_{Py} and X_{Sps} (and X_{Alm}) are more consistent with lower (re)equilibration temperatures, which probably are a function of the smaller grain size. The maximum X_{Py} corresponds to retrograde re-equilibration at around 700°C. Concentrations of X_{Gr}, which are similar throughout the grain, correspond to those predicted at the peak of metamorphism.

Tectonic implications of the *P–T* paths from the Vilaine Group metapelites and the SBMB migmatites

On the basis of age data summarized by Brown & Dallmeyer (1996), we infer that the Vilaine Group and the SBMB probably had a coupled prograde and retrograde evolution. Figure 10 is a summary diagram to show *P–T* paths for both the Vilaine Group and the SBMB. A prograde decompression segment for the former is inferred based on the evidence from the latter. Given the evidence for cation equilibration in garnet in the Vilaine rocks, any evidence for this segment is likely to have been erased and our interpretation is conjectural. Although complicated by the prograde decompression segment, the two *P–T* paths are essentially nested, consistent with a common tectonometamorphic evolution.

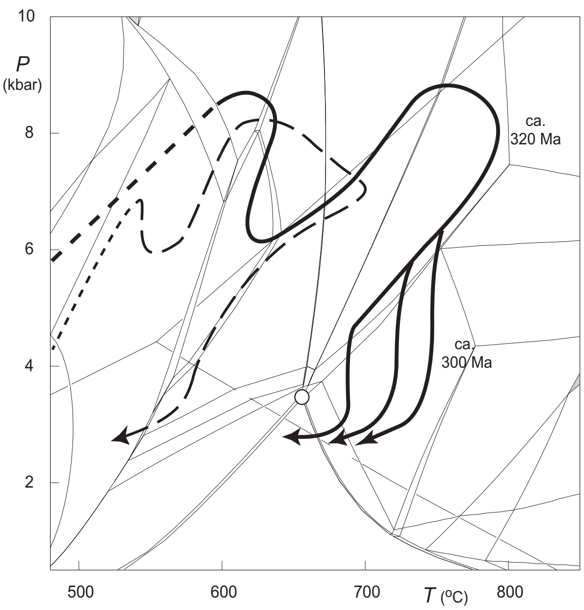

Fig. 10. Summary diagram illustrating possible *P–T* paths for the metapelitic rocks of the Vilaine estuary (dashed curve) and the SBMB (continuous curve), including the inferred timing of the metamorphic peak and the retrograde decompression segment. The implied *T* of the decompression segment is a function of the degree of net melt loss.

The Belle-Ile Group forms an upper structural unit that preserves a record of Late Devonian peak metamorphism in a subduction-zone environment, and subsequent Early Carboniferous exhumation and cooling by *ca.* 350 Ma (Bosse *et al.*, 2000; Le Hébel, 2002). We suggest that exhumation of the Belle-Ile Group probably occurred synchronously with burial of the Vilaine Group and the protolith of the SBMB. Furthermore, it is likely that subduction was terminated as Gondwanan continental lithosphere progressively choked the subduction zone during burial of the Vilaine Group and the protoliths of the SBMB.

Burial of the lower structural units is inferred to have occurred in two stages, as evidenced by the complex prograde *P–T* path derived from the SBMB rocks. For the migmatites, the *P–T* path shows burial to about 9 kbar followed by exhumation to about 6 kbar, before a second burial to about 9 kbar during heating to equilibrate with a higher geothermal gradient. We infer that this two-stage burial probably affected rocks of the Vilaine Group as well. During the period of prograde heating to peak *T*, slab detachment may have occurred (Brown & Dallmeyer, 1996), although the relict slab appears to remain beneath Central Armorica (Brun *et al.*, 2002; Judenherc *et al.*, 2002, 2003). This is one mechanism by which heat from the convecting mantle can be brought closer to the crust to drive metamorphism, as asthenospheric inflow is likely to follow slab detachment.

The SBMB is exposed in structural culminations, interpreted to be the result of extension that allowed the mid- and lower-crustal units to rise, initiating several boudin- or dome-like structures (Gapais *et al.*, 1995; Tirel *et al.*, 2003) and forming a core complex (Brown & Dallmeyer, 1996). As the weak melt-bearing crust of the SBMB responded to the regional east–west extension by rising, so the migmatitic layering and fabric were rotated from sub-horizontal to sub-vertical. Pervasive dextral shear related to displacement on the SASZ synchronous with rise of the SBMB facilitated extraction of melt generated during the second, cordierite-producing melting episode (Marchildon & Brown, 2003). Marchildon & Brown (2003) suggested that melt lost at this stage accumulated at the lower contact at the Belle-Ile Group synchronously with extensional detachment. Displacement related to the detachment was recorded by the late-magmatic–early-subsolidus S–C fabrics present in the Quiberon, Sarzeau and Guérande plutons (Bouchez *et al.*, 1981; Audren, 1987; Gapais *et al.*, 1993; Brown & Dallmeyer, 1996).

CONCLUSIONS

Extant studies of subsolidus and migmatitic metapelitic rocks from the Variscides of southern Brittany suggest that the rocks followed a clockwise P–T path. Pseudosections constructed in the MnNCKFMASH system for an average subaluminous metapelite bulk composition, and contoured for modal proportions of X_{H}, melt and garnet, and for compositional isopleths of garnet, adequately predict phase and reaction relations that are consistent with those observed in the rocks. The pseudosections are powerful in that they allow additional constraints on the P–T–X evolution that cannot necessarily be educed from thermobarometric calculations.

The subsolidus rocks of the Vilaine Group followed a clockwise P–T path. Successive dehydration reactions along the prograde path produced garnet, kyanite at the pressure peak of around 8 kbar, at 625°C, and sillimanite at peak T (around 7 kbar, 700°C). The retrograde evolution was characterized by the production of staurolite and sillimanite. The former was subsequently replaced by andalusite and biotite, which was in places replaced by phengitic white mica. This retrograde evolution (and implicitly the late development of white mica) implies an external supply of H_2O-rich volatile phase, which we infer was derived from crystallizing granite at deeper structural levels.

Within migmatites, zoned inclusion assemblages in garnet suggest that the subsolidus prograde path included a decompression segment from the kyanite to staurolite with Al_2SiO_5 stability fields; kyanite was the stable phase as the rocks crossed the major VPA muscovite-consuming melting reaction. Peritectic garnet-bearing leucosomes developed at the metamorphic peak of about 8 kbar at 800°C. Following probable net melt loss, retrograde cooling along a P–T path with a shallow to moderate positive $\mathrm{d}P/\mathrm{d}T$ resulted in partial crystallization of the remaining melt and replacement of garnet by biotite and sillimanite by plagioclase and quartz. A period of decompression to around 4 kbar followed, during which sillimanite and biotite, and sometimes garnet, were replaced by cordierite. Porphyroblasts of peritectic cordierite occur within interboudin partitions, suggesting that the decompression step was associated with a second pulse of melt production and net melt loss.

The broad correspondence of the predictions from the pseudosections to thermobarometric estimates is encouraging. When used in conjunction with macro- and microstructural observations (e.g. Triboulet & Audren, 1985, 1988; Jones & Brown, 1990; Audren & Triboulet, 1993) and geochronology (Brown & Dallmeyer, 1996), accurate constraints may be placed on the P–T–t–d evolution of rocks and melt loss from rocks; this allows sophisticated tectonothermal models to be advanced. In the context of southern Brittany, initiation of crustal thinning in response to the start of regional extension may have triggered decompression melting, passive rise of the migmatitic core and continued melting in a feedback relation. Fugitive melt that accumulated in thin, structurally controlled leucogranite plutons may have facilitated the final stage of tectonic exhumation (Gapais *et al.*, 1993; Brown & Dallmeyer, 1996).

ACKNOWLEDGEMENTS

We thank Phil Piccoli for his help with X-ray mapping and element spot analysis, and P. J. O'Brien and R. W. White for reviews that motivated improvements to the paper. We acknowledge support from NSF grant EAR 0003531 and the University of Maryland.

REFERENCES

Atherton, M. P. & Brotherton, M. S. (1982). Major element composition of the pelites of the Scottish Dalradian. *Geological Journal* **17**, 185–221.

Audren, C. (1987). Évolution structurale de la Bretagne méridionale au Paléozoique. *Mémoires de la Société Géologique et Minéralogique de Bretagne* **31**.

Audren, C. & Plaine, J. (1986). *Notice explicative de la feuille Belle-Ile-en-Mer et Iles Houat et Hoedic (Carte Géologique de la France 1:50,000)*. Orleans: BRGM, 38 pp.

Audren, C. & Triboulet, C. (1993). P–T–t–deformation paths recorded by kinzigites during diapirism in the western Variscan Belt (Golfe du Morbihan, southern Brittany, France). *Journal of Metamorphic Geology* **11**, 337–357.

Ballèvre, M., Paris, F. & Robardet, M. (1992). Corrélations ibéro-armoricaines du Paléozoïque: une confrontation des donnés paléobiogéographiques et tectonométamorphiques. *Comptes Rendus de l'Académie des Sciences* **315**, 1783–1798.

Ballèvre, M., Bosse, V. & Féraud, J. (2003*a*). Groix: une île fossile. *Pour la Science* **305**(March), 72–79.

Ballèvre, M., Pitra, P. & Bohn, M. (2003*b*). Lawsonite growth in the epidote blueschist from the Ile de Groix (Armorican Massif, France): a potential geobarometer. *Journal of Metamorphic Geology* **21**, 723–735.

Bernard-Griffiths, J., Peucat, J.-J., Sheppard, S. & Vidal, P. (1985). Petrogenesis of Hercynian leucogranites from the southern Armorican Massif; contribution of REE and isotopic (Sr, Nd, Pb and O) geochemical data to the study of source rock characteristics and ages. *Earth and Planetary Science Letters* **74**, 235–250.

Bernard-Griffiths, J., Carpenter, M. S. N., Peucat, J.-J. & Jahn, B. M. (1986). Geochemical and isotopic characteristics of blueschist facies rocks from the Ile de Groix, Armorican Massif (Northwest France). *Lithos* **19**, 235–253.

Bosse, V., Ballèvre, M., Ferraud, G. & Peucat, J.-J. (2000). Petrological and geochronological constraints on the Ile de Groix blueschist (Armorican Massif, France). In: Diaz Garcia, F., Gonzalez Cuadra, P., Martinez Catalan, J. R. & Arenas, R. (eds) *Variscan–Appalachian Dynamics: the Building of the Upper Palaeozoic Basement. Basement Tectonics, Coruña, Spain, Program and Abstracts* **15**, 63–66.

Bosse, V., Ballèvre, M. & Vidal, O. (2002). Ductile thrusting recorded by the garnet isograd from blueschist-facies metapelites of the Ile de Groix, Armorican Massif, France. *Journal of Petrology* **43**, 485–510.

Bossière, G. (1988). Évolutions chimico-minéralogiques du grenat et de la muscovite au voisinage de l'isograde biotite–staurotide dans un métamorphisme prograde de type barrovien: un exemple en Vendée littorale (Massif Armoricain). *Comptes Rendus de l'Académie des Sciences, Série II* **306**, 135–140.

Bouchez, J.-L., Guillet, P. & Schevalier, F. (1981). Structures d'écoulement liées à la mise en place du granite de Guérande (Loire-Atlantique, France). *Bulletin de la Société Géologique de France* **23**, 387–399.

Brown, M. (1983). The petrogenesis of some migmatites from the Presqu'ile de Rhuys, southern Brittany, France. In: Atherton, M. P. & Gribble, C. D. (eds) *Migmatites, Melting and Metamorphism*. Nantwich: Shiva, pp. 174–200.

Brown, M. (2002). Prograde and retrograde processes in migmatites revisited. *Journal of Metamorphic Geology* **20**, 25–40.

Brown, M. & Dallmeyer, R. D. (1996). Rapid Variscan exhumation and the role of magma in core complex formation: southern Brittany metamorphic belt, France. *Journal of Metamorphic Geology* **14**, 361–379.

Brown, M. & O'Brien, P. J. (1997). Evolution of metamorphic belts: a changing view. In: Qian, X., You, Z. & Hall, H. C. (eds) *Precambrian Geology and Metamorphic Petrology, Proceedings of the 30th International Geological Congress, 17*. Zeist, Netherlands: VSP, pp. 217–231.

Brun, J.-P. & Burg, J.-P. (1982). Combined thrusting and wrenching in the Ibero-Armorican arc: a corner effect during continental collision. *Earth and Planetary Science Letters* **61**, 319–332.

Brun, J.-P., Gapais, D., Gumiaux, C., Granet, M. & Judenherc, S. (2002). Strike-slip induced horizontal shear at the lithosphere base: evidence from the South Armorican Shear Zone. In: *Transport and Flow Processes in Shear Zones, Geological Society, London, 2–3 September, 2002, Program and Abstracts*, p. 13.

Burg, J.-P., Van Den Driessche, J. & Brun, J.-P. (1994). Syn- to post-thickening extension in the Variscan belt of western Europe: modes and structural consequences. *Géologie de la France* **3**, 33–51.

Cagnard, F., Gapais, D., Brun, J.-P., Van den Driessche, J. & Gumiaux, C. (2004). Late-Hercynian pervasive crustal-scale extension in Vendée (Armorican Massif, France). *Journal of Structural Geology* **22**, 235–249.

Carlson, W. D. (2002). Scales of disequilibrium and rates of equilibration during metamorphism. *American Mineralogist* **87**, 185–204.

Carson, C. J., Powell, R. & Clarke, G. L. (1999). Calculated mineral equilibria for eclogites in $CaO–Na_2O–FeO–MgO–Al_2O_3–SiO_2–H_2O$; application to the Pouebo Terrane, Pam Peninsula, New Caledonia. *Journal of Metamorphic Geology* **17**, 9–24.

Cesare, B., Marchesi, C., Hermann, J. & Gomez-Pugnaire, M. T. (2003). Primary melt inclusions in andalusite from anatectic graphitic metapelites; implications for the position of the Al_2SiO_5 triple point. *Geology* **31**, 573–576.

Chernoff, C. B. & Carlson, W. D. (1997). Disequilibrium for Ca during growth of pelitic garnet. *Journal of Metamorphic Geology* **15**, 421–438.

Connolly, J. A. D. & Cesare, B. (1993). C–O–H–S fluid composition and oxygen fugacity in graphitic metapelites. *Journal of Metamorphic Geology* **11**, 379–388.

Dalrymple, D. J. (1995). Contact anatexis of Dalradian metapelites from the Huntly–Knock area, Aberseenshire, N. E. Scotland. Ph.D. thesis, University of Manchester.

Djro, S. C., Triboulet, C. & Audren, C. (1989). Les chemins pression–température–temps–déformation–espace (P–T–t–d–e) dans les micaschistes associés aux schistes bleus de l'île de Groix, Bretagne Méridionale, France. *Schweizerische Mineralogische und Petrographische Mitteilungen* **69**, 73–90.

Gapais, D. & Le Corre, C. (1980). Is the Hercynian belt of Brittany a major shear zone? *Nature* **288**, 574–576.

Gapais, D., Lagarde, J. L., Le Corre, C., Audren, C., Jegouzo, P., Casas Sainz, A. & Van Den Driessche, J. (1993). La zone de cisaillement de Quiberon: temoin d'extension de la chaîne varisque en Bretagne meridionale au Carbonifère. *Comptes Rendus de l'Académie des Sciences* **316**, 1123–1129.

Gapais, D., van den Driessche, J., Brun, J.-P. & Richer, C. (1995). Pervasive ductile spreading and boudinage in extending orogens; evidence from the French Variscan Belt. *Terra Abstracts* **7**, 121.

Goujou, J. C. (1992). Analyse pétro-structurale dans un avant-pays métamorphique: influence du plutonisme tardi-orogénique varisque sur l'encaissant épi- à mésozonal de Vendée. *Documents du BRGM* **216**, 347 pp.

Guiraud, M., Burg, J.-P. & Powell, R. (1987). Evidence for a Variscan suture zone in the Vendee, France; a petrological study of blueschist facies rocks from Bois de Cené. *Journal of Metamorphic Geology* **5**, 225–237.

Guiraud, M., Powell, R. & Rebay, G. (2001). H_2O in metamorphism and unexpected behaviour in the preservation of metamorphic mineral assemblages. *Journal of Metamorphic Geology* **19**, 445–454.

Harley, S. L. & Carrington, D. P. (2001). The distribution of H_2O between cordierite and granitic melt; H_2O incorporation in cordierite and its application to high-grade metamorphism and crustal anatexis. *Journal of Petrology* **42**, 1595–1620.

Hensen, B. J. (1971). Theoretical phase relations involving cordierite and garnet in the system $MgO–FeO–Al_2O_3–SiO_2$. *Contributions to Mineralogy and Petrology* **33**, 191–214.

Holland, T. J. B. & Powell, R (1996*a*). Thermodynamics of order–disorder in minerals 1: symmetric formalism applied to minerals of fixed composition. *American Mineralogist* **81**, 1413–1424.

Holland T. J. B. & Powell, R. (1996*b*). Thermodynamics of order–disorder in minerals 2: symmetric formalism applied to solid solutions. *American Mineralogist* **81**, 1425–1437.

Holland, T. J. B. & Powell, R. (1998). An internally consistent thermodynamic data set for phases of petrological interest. *Journal of Metamorphic Geology* **16**, 309–343.

Holland, T. J. B. & Powell, R. (2001). Calculation of phase relations involving haplogranite melts using an internally consistent dataset. *Journal of Petrology* **42**, 673–683.

Holland, T. J. B. & Powell, R. (2003). Activity–composition relations for phases in petrological calculations: an asymmetric multicomponent formulation. *Contributions to Mineralogy and Petrology* **142**, 492–501.

Johnson, T. E., Brown, M. & Solar, G. S. (2003*a*). Low-pressure subsolidus and suprasolidus phase equilibria in the MnNCKFMASH system: constraints on conditions of regional metamorphism in western Maine, northern Appalachians. *American Mineralogist* **88**, 624–638.

Johnson, T. E., Gibson, R. L., Brown, M., Buick, I. S. & Cartwright, I. (2003*b*). Partial melting of metapelitic rocks beneath the Bushveld Complex, South Africa. *Journal of Petrology* **44**, 789–813.

Jones, K. A. (1991). Palaeozoic continental margin tectonics in southern Armorica. *Journal of the Geological Society, London* **148**, 55–64.

Jones, K. A. & Brown, M. (1989). The metamorphic evolution of the southern Brittany Migmatite Belt. In: Daly, J. S., Cliff, R. A. & Yardley, B. W. D. (eds) *Evolution of Metamorphic Belts. Geological Society, London, Special Publications* **43**, 501–505.

Jones, K. A. & Brown, M. (1990). High-temperature 'clockwise' P–T paths and melting in the development of regional migmatites: an example from southern Brittany, France. *Journal of Metamorphic Geology* **8**, 551–578.

Judenherc, S., Granet, M., Brun, J.-P., Poupinet, G., Plomerová, J., Mocquet, A. & Achauer, U. (2002). Images of lithospheric heterogeneities in the Armorican segment of the Hercynian Range in France. *Tectonophysics* **358**, 121–143.

Judenherc, S., Granet, M., Brun, J.-P. & Poupinet, G. (2003). The Hercynian collision in the Armorican Massif; evidence of different lithospheric domains inferred from seismic tomography and anisotropy. *Bulletin de la Société Géologique de France* **174**, 45–57.

Kelsey, D. E., White, R. W. & Powell, R. (2003*a*). Orthopyroxene–sillimanite–quartz assemblages: distribution, petrology, quantitative P–T–X constraints and P–T paths. *Journal of Metamorphic Geology* **21**, 439–453.

Kelsey, D. E., White, R. W., Powell, R., Wilson, C. J. L. & Quinn, C. D. (2003*b*). New constraints on metamorphism in the Rauer Group, Prydz Bay, east Antarctica. *Journal of Metamorphic Geology* **21**, 739–759.

Kretz, R. (1983). Symbols for rock-forming minerals. *American Mineralogist* **68**, 277–279.

Le Hébel, F. (2002). Déformation continentale et histoire des fluides au cours d'un cycle subduction, exhumation, extension. Exemple des Porphyroïdes sud-armoricains. Ph.D. thesis, University of Rennes I.

Le Hébel, F., Gapais, D., Fourcade, S. & Capdevila, R. (2002*a*). Fluid-assisted large strains in a crustal-scale décollement (Hercynian belt of south Brittany, France). In: De Meer, S., Drury, M.R., De Bresser, J. H. P. & Pennock, G. M. (eds) *Deformation Mechanisms, Rheology and Tectonics: Current Status and Future Perspectives. Geological Society, London, Special Publications* **200**, 85–101.

Le Hébel, F., Vidal, O., Kienast, J. R. & Gapais, D. (2002*b*). Les 'Porphyroïdes' de Bretagne méridionale: une unité de HP–BT dans la chaîne hercynienne. *Comptes Rendus Geoscience* **334**, 205–211.

Mahar, E. M., Baker, J. M., Powell, R., Holland, T. J. B. & Howell, N. (1997). The effect of Mn on mineral stability in metapelites. *Journal of Metamorphic Geology* **15**, 223–238.

Marchildon, N. & Brown, M. (2003). Spatial distribution of melt-bearing structures in anatectic rocks from Southern Brittany, France: implications for melt transfer at grain- to outcrop-scale. *Tectonophysics* **364**, 215–325.

Marmo, B. A., Clarke, G. L. & Powell, R. (2002). Fractionation of bulk rock composition due to porphyroblast growth: effects on eclogite facies mineral equilibria, Pam Peninsula, New Caledonia. *Journal of Metamorphic Geology* **20**, 151–165.

Matte, P. (1991). Accretionary history and crustal evolution of the Variscan belt of Europe. *Tectonophysics* **196**, 309–337.

Matte, P. (2001). The Variscan collage and orogeny (480–290 Ma) and the definition of the Armorica microplate: tectonic approach. *Terra Nova* **13**, 122–128.

Matte, P. & Hirn, A. (1988). Seismic signature and tectonic cross section of the Variscan Belt in western France. *Tectonics* **72**, 141–155.

Pattison, D. R. M. (1992). Stability of andalusite and sillimanite and the Al_2SiO_5 triple point: constraints from the Ballachulish aureole, Scotland. *Journal of Geology* **100**, 423–446.

Pattison, D. R. M. & Tracy, R. J. (1991). Phase equilibria and thermobarometry of metapelites. In: Kerrick, D. M. (ed.) *Contact Metamorphism. Mineralogical Society of America, Reviews in Mineralogy* **26**, 105–206.

Pattison, D. R. M., Spear, F. S. & Cheney, J. T. (1999). Polymetamorphic origin of muscovite + cordierite + staurolite + biotite assemblages: implications for the metapelitic petrogenetic grid and for P–T paths. *Journal of Metamorphic Geology* **17**, 685–703.

Pattison, D. R. M., Chacko, T., Farquhar, J. & McFarlane, C. R. M. (2003). Temperatures of granulite-facies metamorphism: constraints from experimental phase equilibria and thermobarometry corrected for retrograde exchange. *Journal of Petrology* **44**, 867–900.

Powell, R. & Downes, J. (1990). Garnet porphyroblast-bearing leucosomes in metapelites: mechanisms, phase diagrams, and an example from Broken Hill, Australia. In: Ashworth, J. R. & Brown, M. (eds) *High-Temperature Metamorphism and Crustal Anatexis*. London: Unwin, pp. 105–123.

Powell, R. & Holland, T. J. B. (1988). An internally consistent thermodynamic dataset with uncertainties and correlations. III. Application methods, worked examples and a computer program. *Journal of Metamorphic Geology* **6**, 173–204.

Powell, R. & Holland, T. J. B. (1994). Optimal geothermometry and geobarometry. *American Mineralogist* **79**, 120–133.

Quinquis, H. & Choukroune, P. (1981). Les schistes bleus de l'île de Groix dans la chaîne hercynienne: implications cinématiques. *Bulletin de la Société Géologique de France* **23**, 409–418.

Schultz, B., Triboulet, C., Audren, C., Pfeifer, H.-R. & Gilg, A. (2001). Two-stage prograde and retrograde Variscan metamorphism of glaucophane-eclogites, blueschists and greenschists from the Ile de Groix (Brittany, France). *International Journal of Earth Sciences* **90**, 871–889.

Schultz, B., Audren, C. & Triboulet, C. (2002). Oxygen isotope record of fluid–rock–SiO_2 interaction during progressive deformation and quartz veining in the meta-volcanosediments of Belle-Ile (Southern Brittany). *Journal of Structural Geology* **24**, 1281–1297.

Senior, A. & Leake, B. E. (1978). Regional metasomatism and the geochemistry of the Dalradian metasediments of Connemara, western Ireland. *Journal of Petrology* **19**, 585–625.

Shaw, D. M. (1956). Geochemistry of pelitic rocks. Part III: Major elements and general geochemistry. *Geological Society of America Bulletin* **67**, 919–934.

Shelley, D. & Bossière, G. (1999). Ile de Groix: retrogression and structural developments in an extensional régime. *Journal of Structural Geology* **21**, 1441–1455.

Solar, G. S. & Brown, M. (2001). Petrogenesis of migmatites in Maine, USA. Possible source of peraluminous granite in plutons. *Journal of Petrology* **42**, 789–823.

Spear, F. S. & Daniel, C. G. (2001). Diffusion control of garnet growth, Harpswell Neck, Maine, USA. *Journal of Metamorphic Geology* **19**, 179–195.

Spear, F. S., Kohn, M. J. & Cheney, J. T. (1999). P–T paths from anatectic pelites. *Contributions to Mineralogy and Petrology* **134**, 17–32.

Stüwe, K. (1997). Effective bulk composition changes due to cooling: a model predicting complexities in retrograde reaction textures. *Contributions to Mineralogy and Petrology* **129**, 43–52.

Tinkham, D. K. (2002). MnNCKFMASH metapelite phase equilibria, garnet activity modeling, and garnet Sn–Nd chronology: applications to the Waterville Formation, Maine, and south–central Nason Terrane, Washington. Ph.D. thesis, University of Alabama, Tuscaloosa.

Tinkham, D. K., Zuluaga, C. A. & Stowell, H. H. (2001). Metapelitic phase equilibria modelling in MnNCKFMASH: the effect of variable Al_2O_3 and MgO/(MgO + FeO) on mineral stability. *Geological Materials Research* **3**, 1–42.

Tirel, C., Brun, J.-P. & Burov, E. (2003). Thermo-mechanical modelling of extensional gneiss domes. In: *Deformation Mechanisms, Rheology and Tectonics, Gésciences, Rennes, St. Malo, France, 14–16 April 2003, Abstract Volume*, p. 160.

Tracy, R. J., Robinson, P. & Thompson, A. B. (1976). Garnet composition and zoning in the determination of temperature and pressure of metamorphism, central Massachusetts. *American Mineralogist* **61**, 762–775.

Triboulet, C. (1974). Les glaucophanites et roches associées de l'île de Groix (Morbihan, France): étude minéralogique et pétrogénétique. *Contributions to Mineralogy and Petrology* **45**, 65–90.

Triboulet, C. (1991). Étude géothermo-barométrique comparée des schistes bleus paléozoïques de l'Ouest de la France (Ile de Groix, Bretagne méridionale et Bois de Cené, Vendée). *Comptes Rendus de l'Académie des Sciences, Série II* **312**, 1163–1168.

Triboulet, C. & Audren, C. (1985). Continuous reactions between biotite, garnet, staurolite, kyanite–sillimanite–andalusite and P–T–time–deformation path in micaschists from the estuary of the river Vilaine, South Brittany, France. *Journal of Metamorphic Geology* **3**, 91–105.

Triboulet, C. & Audren, C. (1988). Controls on P–T–t deformation path from amphibolite zonation during progressive metamorphism of basic rocks (estuary of the River Vilaine, South Brittany, France). *Journal of Metamorphic Geology* **6**, 117–133.

White, R. W. & Powell, R. (2002). Melt loss and the preservation of granulite facies mineral assemblages. *Journal of Metamorphic Geology* **20**, 621–632.

White, R. W., Powell, R., Holland, T. J. B. & Worley, B. (2000). The effect of TiO_2 and Fe_2O_3 on metapelitic assemblages at greenschist and amphibolite facies conditions: mineral equilibria calculations in the system K_2O–FeO–MgO–Al_2O_3–SiO_2–H_2O–TiO_2–Fe_2O_3. *Journal of Metamorphic Geology* **18**, 497–511.

White, R. W., Powell, R. & Holland, T. J. B. (2001). Calculation of partial melting equilibria in the system Na_2O–CaO–K_2O–FeO–MgO–Al_2O_3–SiO_2–H_2O (NCKFMASH). *Journal of Metamorphic Geology* **19**, 139–153.

White, R. W., Powell, R. & Clarke, G. L. (2002). The interpretation of reaction textures in Fe-rich metapelitic granulites of the Musgrave Block, central Australia: constraints from mineral equilibria calculations in the system K_2O–FeO–MgO–Al_2O_3–SiO_2–H_2O–TiO_2–Fe_2O_3. *Journal of Metamorphic Geology* **19**, 139–153.

Zeh, A. & Holness, M. (2003). The effect of reaction overstep on garnet microtextures in metapelitic rocks of the Ilesha Schist Belt, SW Nigeria. *Journal of Petrology* **44**, 967–994.